A SUMMARY OF THE SUBMARINE GROUNDWATER DISCHARGE (SGD) IN KAHANA BAY: SPATIAL AND INTRA-DAILY VARIABILITY

A THESIS SUBMITTED TO
THE GLOBAL ENVIRONMENTAL SCIENCE
UNDERGRADUATE DIVISION IN PARTIAL FULFILLMENT
OF THE REQUIREMENTS FOR THE DEGREE OF

BACHELOR OF SCIENCE

IN

GLOBAL ENVIRONMENTAL SCIENCE

MAY 2013

By
Kimberley K. Mayfield

Thesis Advisors

Henrieta Dulaiova
Craig Glenn

We certify that we have read this thesis and that, in our opinion, it is satisfactory in scope and quality as a thesis for the degree of Bachelor of Science in Global Environmental Science.

THESIS ADVISORS

_____

Henrieta Dulaiova
Department of Geology and Geophysics

_____

Craig Glenn
Department of Geology and Geophysics

ACKNOWLEDGMENTS

I would firstly like to thank my research advisors, Henrieta Dulaiova and Craig Glenn, and academic advisor, Jane Schoonmaker, for their guidance, support, patience, and encouragement over these past four years. Secondly, I'd like to thank the other SGD team members: Jacque Kelly, Christine Waters, and Joseph Fackrell, who have each been invaluable mentors that volunteered their guidance, time, and assistance throughout the mapping, field, laboratory, and analysis stages of this project.

This paper is funded in part by a grant/cooperative agreement from the National Oceanic and Atmospheric Administration, Project R/HE-2, which is sponsored by the University of Hawaii Sea Grant College program, SOEST, under Institutional Grant No. NA09OAR4170060 from NOAA Office of Sea Grant, Department of Commerce. The views expressed herein are those of the author and do not necessarily reflect the views of NOAA or any of its subagencies. UNIHI-SEAGRANT-XB-12-01.

The Center for Microbial Oceanography and Education Scholars Program also provided academic and financial support for this project, for which I am truly grateful. I would also like to thank EPSCoR for its financial support of other field expeditions that I partook in, which taught me how to conduct SGD research.

Additionally, I would be remiss to not thank the Wallace `ohana for their hospitality and assistance during the field work segment of this research, Matt Barbee for his assistance in data acquisition and mapping, as well as Shellie Habel for her patient and helpful edits to this manuscript.

ABSTRACT

From global to local scales, submarine groundwater discharge (SGD) is a significant conduit through which nutrients and contaminants may be transported to the coastal ocean. Therefore, it is important that SGD inputs to coastal marine environments be located, quantified, and understood fully. This study utilizes a combination of different SGD research techniques to establish a comprehensive research methodology for SGD studies that can provide a regional-scale understanding of SGD, quantify its flux to coastal waters, and the nutrient fluxes derived from SGD inputs. Kahana Bay, a semi-protected embayment on the northeastern shore of O`ahu, Hawai`i, was selected as the field site for this study because its watershed is an important hydrologic resource, and the bay itself is a known conduit of this watershed's SGD.

Due to the relatively cool temperature of groundwater with respect to overlying seawater, the surface water expression of SGD in Kahana Bay was first mapped using high-resolution airborne thermal infrared (TIR) remote sensing. After identifying potential SGD in the TIR map, an in situ survey was conducted of the surface waters around the perimeter of the bay for ^{222}Rn activities – a geochemical tracer for SGD. Based on a coastal ^{222}Rn mass balance, we calculated a total SGD flux to Kahana Bay of 62,736 m^3/day. Using piezometer data from coastal sediments, we also determined that about 30% (18,820 m^3/day) of the SGD is freshwater. Huilua Fishpond, on the eastern edge of Kahana Bay, is calculated here to account for ~63% of the bay's total SGD.

Time series data from the eastern shore of Kahana Bay were used to determine the intra-daily variability of SGD with respect to tidal fluctuations and the effects this variability has on coastal salinity and pH. Average dissolved nutrient concentrations in

groundwater samples were multiplied by the SGD flux to estimate the SGD-derived nutrient fluxes to Kahana Bay. Dissolved nutrient data were also collected from Kahana Stream and ratios of nutrients derived from SGD:stream were calculated to be approximately 4:1 for TDN, 5:1 for TDP, and 1:1 for silica (Si). Both the volumetric SGD and nutrient fluxes calculated in this study are in agreement with previous ^{222}Rn/nutrient findings from the benthic seepage meter studies of Garrison et al. (2003).

TABLE OF CONTENTS

LIST OF TABLES

LIST OF FIGURES

CHAPTER 1

INTRODUCTION

1.1 Submarine Groundwater Discharge

Submarine groundwater discharge (SGD) is water, of any chemical composition, that flows from a terrestrial aquifer, through coastal submarine geologic substrate, and into the overlying ocean (Burnett et al., 2003a). This process is driven by precipitation in a watershed that infiltrates into the aquifers, and flows down the hydrological gradient. These processes, along with wave set-up, tidal pumping, and large-scale ocean circulation also affect the amount and composition of SGD. The length of time that the groundwater spends within the terrestrial system depends on a variety of geologic and spatial factors, including - but not limited to - the porosity of the lithology, slope gradient, location of precipitation source, and the presence of any geologic layers with reduced permeability (Gingerich & Oki, 2000). Over a period of time, the groundwater enters into a state of equilibrium with the lithology of the aquifer that is proportional to the solubility of the different geochemical constituents (Morland et al., 1998). In addition to naturally acquired chemical signatures, anthropogenic contamination may enter the groundwater aquifer. Lacking an estuarine filter, this unique geochemical signature can be preserved all the way until groundwater discharges into the ocean and can then be used to locate areas with SGD and non-point source pollution (Dulaiova et al., 2010). This geochemical signature is typically characterized by increased solute or ion concentrations, including common ions, trace metals, some radioactive isotopes, high nutrient content, salinity usually less than that of the overlying ocean, and chemical contamination reflecting the watershed's land uses (Niencheski et al., 2007). SGD's recognition as a potentially

significant contributor to the marine environment's chemical budget is why it has become a topic of growing interest (Taniguchi et al., 2002). Previous research has shown that SGD has the potential to have an equal or greater impact on local marine chemistry and biological growth in coastal waters than surface water inputs (Johannes et al., 1985, Costa et al., 2008, and Waska & Kim, 2011). In addition, SGD has even been shown to be a significant component of the freshwater flux in the global hydrological cycle. Zekster (2000), for example, estimated that fresh SGD accounts for <10% of surface discharge, but total (fresh- and saltwater discharge) is of much larger magnitude. In addition, total SGD is estimated to contribute between 0.80 – 1.60 times the freshwater inputs of rivers to the Atlantic Ocean (Moore et al., 2008). These examples illustrate that it is important to accurately locate and quantify such a potentially significant chemical input to coastal marine systems on a variety of scales.

1.2 O`ahu

The island of O`ahu is the second oldest of the six main islands of the Hawaiian Island chain. With 70% of the state's population residing on O`ahu, it is also the most developed and urbanized (U.S. Census, 2012). O`ahu was created by two volcanic ediphices – the Waianae on the west side, and Ko`olau on the east – with basalt ages ranging from Pliocene to Holocene in age (Miller, 1999). This basaltic rock comprises the majority of the islands' aquifers. The island also has a significant amount of consolidated, Quaternary-age sedimentary deposits. These deposits, primarily consisting of coralline limestone, have a tendency to form productive lowland aquifers of a brackish/saltwater composition and are characterized by high hydraulic conductivity rates (Miller, 1999). In areas where these coralline limestone deposits have been partially

dissolved and/or contain large secondary openings, they have been documented as having hydraulic conductivity rates up to 20,000 ft/day (6,096 m/day), which are the highest in the state (Miller, 1999). Sometimes these coralline limestone deposits are underlain by and interbedded with Quaternary-age consolidated sedimentary deposits, such as volcanic alluvial and calcareous reefal deposits, of relatively low permeability (Stearns and Vaksvik, 1935; Takasaki et al., 1969; Hunt, 1996). These relatively impermeable lithologies make up what is known as the "coastal caprock" on O`ahu, which impedes SGD and causes a thickening of the freshwater lens behind it. On O`ahu, this coastal caprock is found in Kahuku (the most northeastern watershed) and is extensive along the north-central, southern, and southeastern portions of the island (Stearns and Vatsvik, 1935; Miller, 1999).

1.3 Kahana Bay

1.3.1 Background

Kahana Bay is an example of a semi-protected, Hawaiian marine embayment on the northeastern shore of O`ahu (see Figure 1.1), which is documented to have significant SGD inputs to the bay (Garrison et al., 2003). Compared to the coastal waterbodies surrounding urbanized southern O`ahu, Kahana Bay itself is relatively undisturbed and sheltered. The floor of Kahana Bay is made up of Pleistocene – recent age coral-algal reef and a sediment-filled pre-Pleistocene age paleochannel. This paleochannel formed during the last interglacial stage under relatively low sea level conditions and extends from the middle of the bay out into the ocean (Coulbourn, 1971; Coulbourn et al., 1974).

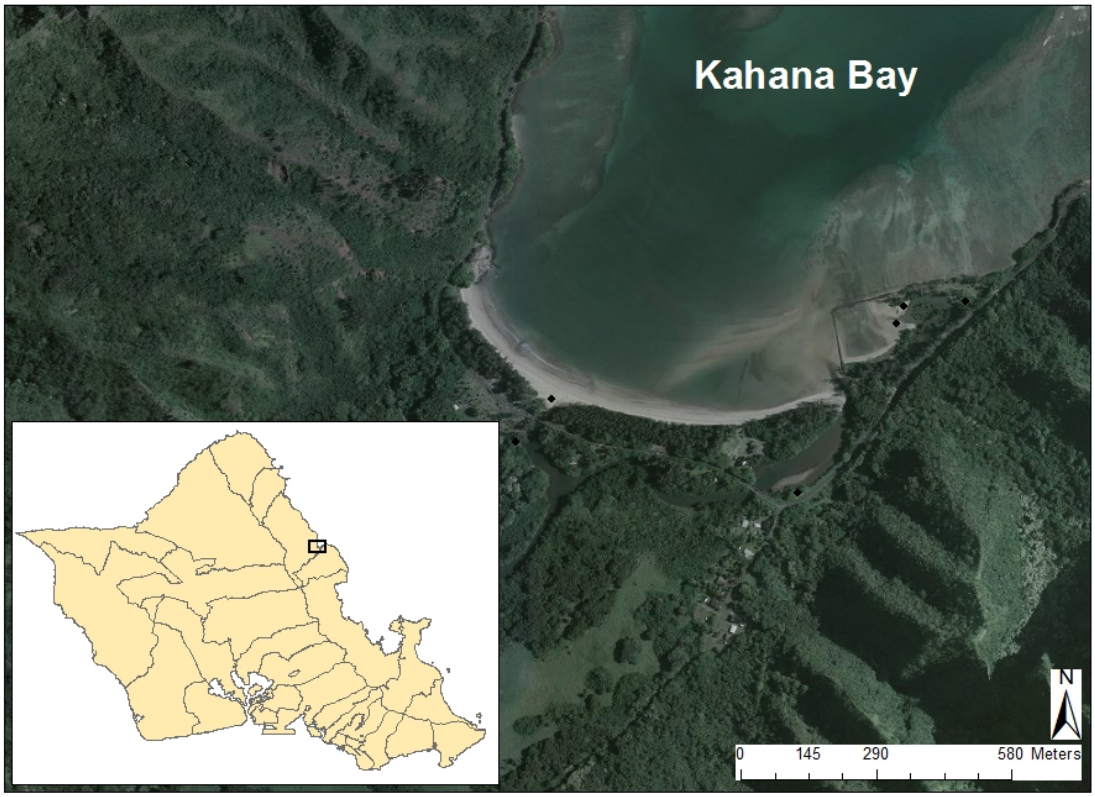

Figure 1.1: A reference map of Kahana Bay with respect to O`ahu

Kahana Bay serves as the receiving waterbody for Kahana Valley, which extends 6.44 km into the Ko`olau mountain range from the shoreline. It receives over 500 cm of rainfall annually, qualifying it as the wettest valley on O`ahu (Takasaki et al., 1969). The geology of Kahana Valley can be broken up into three distinct geologic units: upland Ko`olau basalts, a basaltic, confining lowland sedimentary layer of weathered volcanic talus and Pleistocene-age alluvium, and a younger, less lithified sedimentary coastal overlying unit of Holocene alluvium and calcareous marine sands (see Figure 1.2). The Ko`olau basalts that characterize the Ghyben-Herzberg aquifer of eastern O`ahu and make up the majority of Kahana Valley are often dike-filled and have a range of hydraulic transmissivities from 0.0003 - 0.002 m^2/sec (Takasaki et al., 1969). The confining sedimentary layer of lower Kahana Valley is at least Pleistocene-age (Garrison

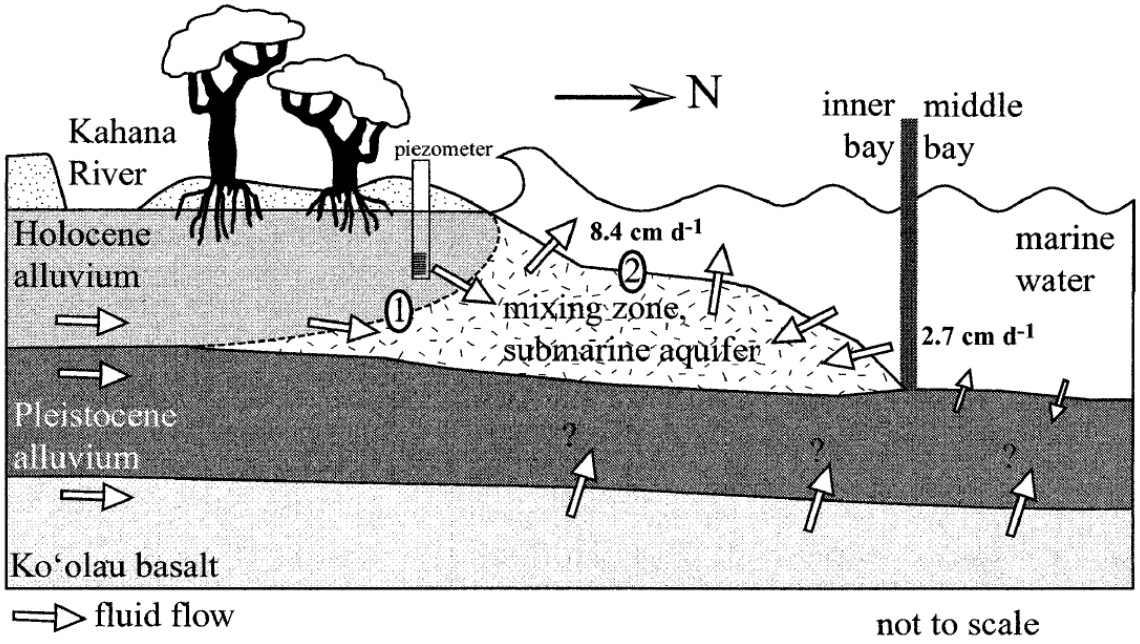

Figure 1.2: A conceptualized cross section of a shore-normal transect of Kahana's coast with the inferred pathways of subsurface flow labeled as arrows from Garrison et al. (2003)

et al., 2003) and is comprised of weathered basaltic talus and alluvium with transmissivities on the order of 10^{-6} m^2/sec (Takasaki et al., 1969). Finally, Kahana's coastal geologic unit, made up of Holocene-age terrestrial alluvium and calcareous sands, is estimated to have transmissivities slightly greater than the lowland sedimentary layer due to the relatively high porosity and low lithification (Garrison et al., 2003).

In addition to its wealth of hydrologic resources, Kahana also has a rich cultural history with a variety of previous land uses. Prior to western contact, Kahana Valley was used as a fishing and farming community; the valley floor was dominated by ponded fields of taro (*Colocasia esculenta*) that were irrigated by water from the valley's streams (DLNR, 2012). On the eastern edge of Kahana Bay, there is a traditional mixohaline Hawaiian fishpond, named Huilua Fishpond, which is fed by a freshwater spring. It is thought to have been built between 1400 – 1600 BCE, long before western contact

(DLNR, 2012). Post western contact, the population of Kahana Valley decreased drastically and the land was converted to commercial sugar cane fields in the early 1900s. During the WWII era, Kahana was converted into a jungle warfare-training site by the military (DLNR, 2012). Currently, the valley is part of a state park and is home to a small residential population. After suffering damage from several tsunamis, the Huilua Fishpond's L-shaped seawall was restored by the state to its historical integrity in 1993 and is now primarily treated as a cultural resource, with only a few recreational fishermen visiting it regularly.

1.3.2 Huilua Fishpond

Huilua Fishpond, as mentioned previously in §1.3.1, is a traditional mixohaline Hawaiian fishpond on the eastern edge of Kahana Bay (see Figure 1.3). It is separated from the bay by an L-shaped, 152 m long traditional lava rock seawall on its western and northern edges. Some sections of the wall are collapsed or loosely piled, allowing for hydrologic exchange between the bay and the fishpond. The fishpond's depth fluctuates with the mixed semi-diurnal tidal range of Kahana Bay. However, some wave energy is dissipated, thereby preventing it from entering the fishpond and shielding the fishpond from much wave action.

Figure 1.3: Huilua Fishpond, circa 1980 (DLNR, 2012)

1.3.3 Previous Research

Two approaches have been previously utilized to estimate the volumetric contribution of SGD to Kahana Bay – a terrestrially based, steady state water budget calculation and a marine-based, observational approach. The earliest two studies of Kahana's hydrologic resources, conducted by Takasaki et al. (1969) and Lau (1973), used a terrestrial-based hydrologic method. This method estimates the SGD flow rate based on average precipitation, river flow, and runoff data from Kahana Valley.

Takasaki estimated that, of the valley's average 60 mgd (2.27×10^5 m^3/day) of precipitation, only about 10 mgd (3.8×10^4 m^3/day) percolated through the ground and was discharged at or near the shoreline. Lau's hydrologic budget used precipitation data

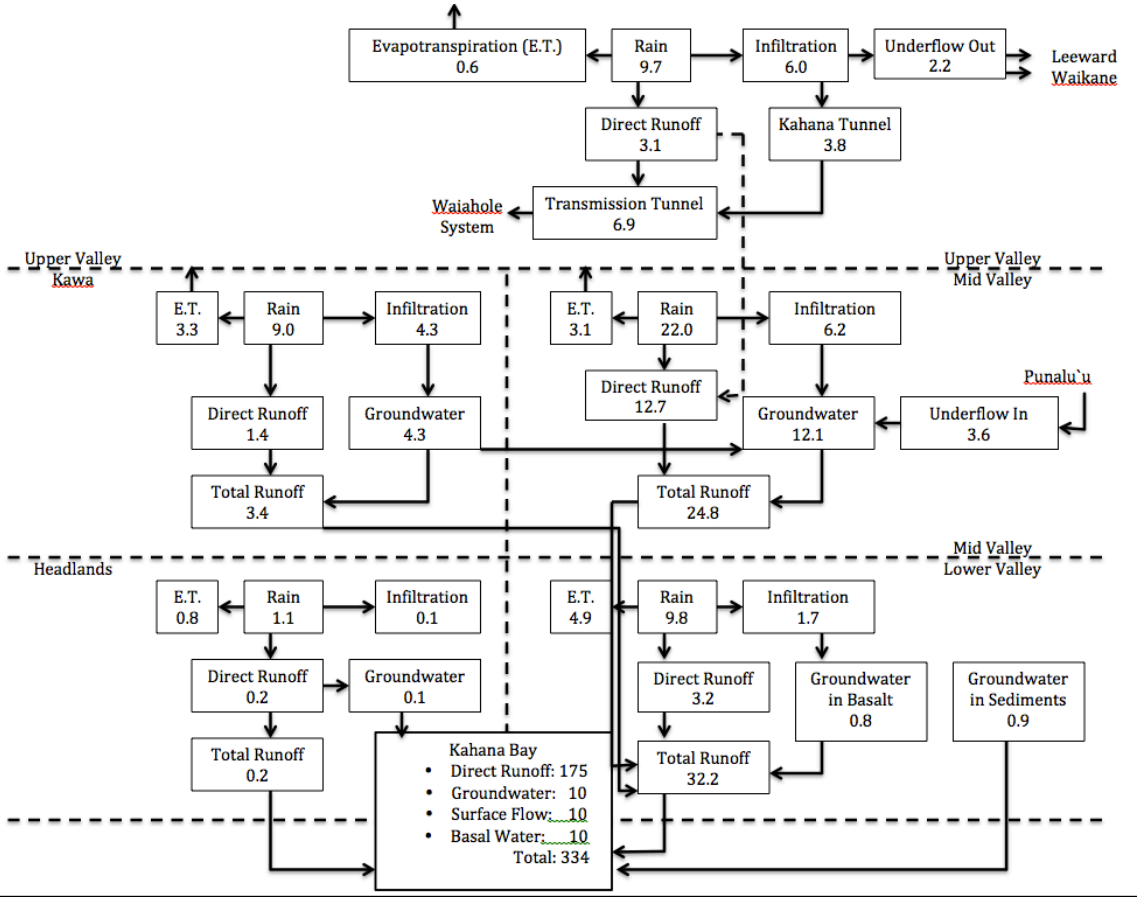

Figure 1.4: A flowchart quantifying the flow of hydrologic resources throughout the Kahana watershed, adapted from a study conducted by Lau in 1973. The groundwater flux to Kahana Bay via groundwater discharge is shown at the bottom to be 10 MGD (approx. 37,854 m^3/day).

recorded over a 40-year period at three USGS rain gauges located throughout the valley and stream flow data from the same USGS gauge that was used in this study (USGS rain gauge #16296500). Lau estimated the groundwater flux to the ocean to be approximately 4 x 10^3 m^3/day (see Figure 1.4 above), nearly an order of magnitude less than Takasaki had estimated four years prior.

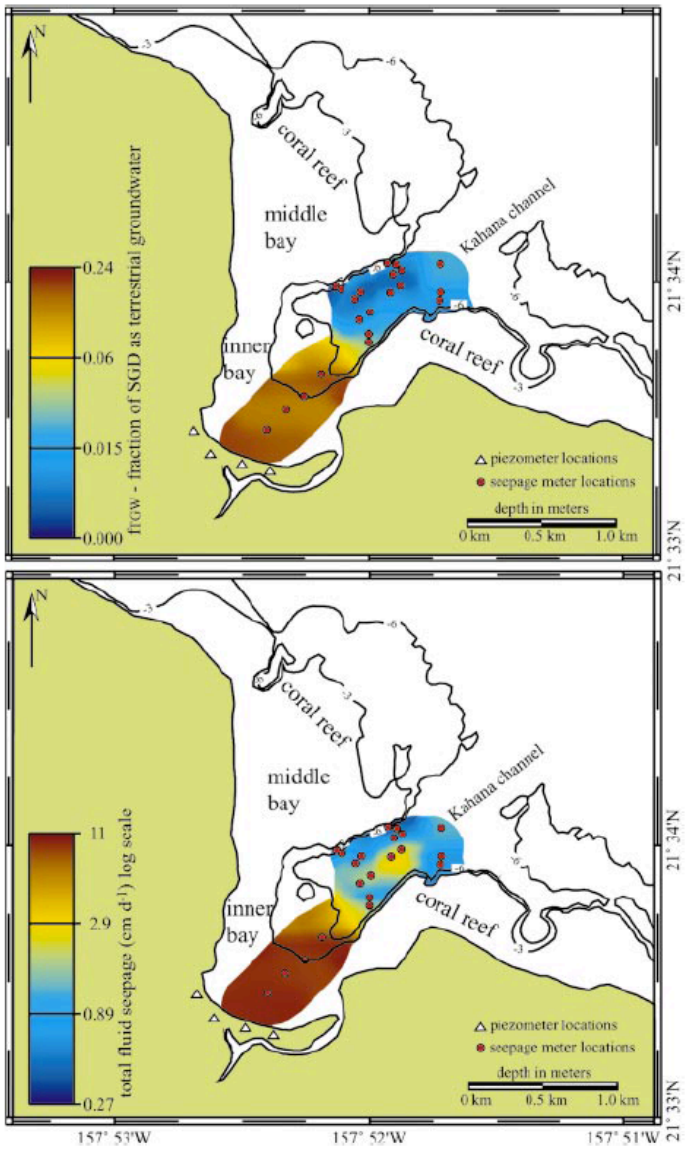

Figure 1.5: Two contour maps from Garrison et al. (2003) that depict total SGD (bottom) and the terrestrial groundwater – derived fraction (above), with sampling locations displayed as red circles and piezometers as white triangles.

In 2003, a study of Kahana Bay was conducted by Garrison et al. (2003) that calculated the volumetric SGD flux to Kahana Bay to be ~90,000 m^3/day using seepage meters and geochemical tracers, such as radioactive ^{222}Rn, Si, and Cl^-. These tracers were used to calculate that 16% of this flow was fresh in its composition and derived from the meteoric groundwater lens. The remaining 84% consisted of recirculated seawater. The majority of SGD was detected along the paleochannel in the middle of the bay (see Figure 1.5).

1.4 Rationale and Study Structure

The goal of this study was to provide the most comprehensive summary of SGD in Kahana Bay to date and demonstrate the benefits of utilizing complimentary SGD identification and quantification techniques that can be applied in future studies. As described above, in §1.3.3, terrestrially based hydrologic budgets and a benthic marine-based SGD study using geochemical tracers have all been used to estimate SGD inputs to Kahana Bay. Neither of these methods, however, is able to confidently illustrate the shape and reach that SGD plumes exhibit as they extend into the coastal ocean. To address this limitation, we chose to implement a high resolution, regional-scale aerial thermal infrared (TIR) survey of Kahana Bay prior to the field research component. This TIR map helped us identify probable locations of SGD within the bay, which was useful information to have when planning the fieldwork component of the project and in the analysis of fieldwork results.

A regional-scale TIR map of the northeastern (windward) O`ahu coastline was prepared, prior to fieldwork in Kahana Bay, to provide a map of potential SGD inputs. Kahana Bay was selected as this study's field site because of the readily identifiable cold signatures along its coastline in the TIR map, the valley's abundant rainfall, and wide range of documented SGD flow rates. Due to the relatively cold nature of SGD, it was hypothesized that the cold signatures absent of river inputs in the image were plumes of cold SGD that buoyantly floated at the seawater's surface. After identifying the probable locations of SGD inputs to Kahana Bay, a two-part fieldwork plan was constructed to examine volumetric and chemical SGD inputs on both spatial and temporal scales.

To corroborate the spatial variability of SGD inputs derived from the TIR image, a geochemical tracer signature survey was conducted. We used ^{222}Rn as groundwater tracer. During this survey, a multiparameter water quality probe, ^{222}Rn in water measuring device, and water sampling were utilized to determine the chemical nature of the SGD that was flowing out to the bay. Additionally, a transect across the bay was delineated, across which sampling for nutrient analysis took place. With both the survey and transect data, comprehensive maps of Kahana Bay were created using an inverse distance weighted interpolation strategy in ArcMap 10.0, based on the spatial research of Shepard (1968).

To determine the variability of SGD on a temporal scale, a time series monitoring station was installed for approximately one and a half days (35 hours) in Huilua Fishpond, on the eastern edge of the bay. This location was selected because it had not been previously investigated for SGD, although it did show pronounced cool water indications of SGD in the TIR image. During this time series monitoring, ^{222}Rn activities, water depth, temperature, salinity, pH, and dissolved oxygen content data were recorded. When the salinity and temperature of the water, depth, and ^{222}Rn activities data were combined in a mass balance equation designed by Burnett & Dulaiova (2003), SGD fluxes to the fishpond could be determined over the course of a full tidal cycle period.

1.5 SGD Research Techniques

1.5.1 Thermal Infrared Remote Sensing

Regional-scale TIR imaging is an effective tool for locating SGD and has been used in a variety of studies around the world (Shaban et al. 2005; Duarte et al., 2006; Johnson et al., 2008). The applicability of TIR mapping in SGD studies is dependent on

the temperature contrast between groundwater discharge and seawater. Additionally, these temperature differences must be visible across the surface of the water where the TIR camera can measure them. In Hawai`i, as long as the SGD is less saline than the overlying marine water, it should buoyantly float up to the surface of coastal waters, where an aerial TIR camera can detect its unique temperature signature.

In higher latitudes, SGD can be seasonally warm or cold relative to coastal marine waters and both of these temperature signatures have been used previously in SGD studies as a means of identifying groundwater discharge plumes on a large scale (Miller and Ullman, 2004; Danielescu et al., 2009). In lower latitudes, SGD usually appears cold, compared to the ambient ocean water, year-round in aerial TIR imagery (Johnson et al., 2008; Kelly et al., 2013). The word "usually" is key because, in some geothermally active areas, SGD can appear relatively warm, such as in the study conducted in the Dead Sea by Akawwi et al. (2008). Additionally, in areas with anthropogenic recharge of thermally polluted effluent (e.g., power plants), the SGD signature may be anomalously warm (Brielmann et al., 2009; Kelly et al., 2013). In Kahana Bay's warm subtropical seawater, groundwater discharge to the bay is expected to appear as a relatively cold signature.

1.5.2 ^{222}Rn as a Geochemical Tracer of SGD

Radioactive geochemical tracers, such as radon (^{222}Rn), can be used to estimate SGD fluxes and the mixing rate of groundwater-derived solutes after these have entered the marine system (Charette et al., 2007). ^{222}Rn's application as a geochemical tracer relies on its relatively high abundance in groundwater, relative to ocean water. ^{222}Rn is a chemically conservative gas. ^{222}Rn is an effective indicator of groundwater inputs because its concentrations are 100 – 10,000 greater in groundwater than in surface waters

(Dulaiova and Burnett, 2008). ^{222}Rn is derived from radioactive decay of ^{226}Ra, a member of the ^{238}U decay chain, and a natural chemical constituent of basaltic volcanism (see Figure 1.6 for a flowchart of the radioactive decay path that ^{238}U takes to produce ^{222}Rn). Additionally, its relatively short half-life (3.8 days) and evasion to the atmosphere suggests that any ^{222}Rn identified in marine systems is a product of recent groundwater inputs. This allows for changes in SGD inputs to be identified over relatively short timescales (Charette et al., 2007).

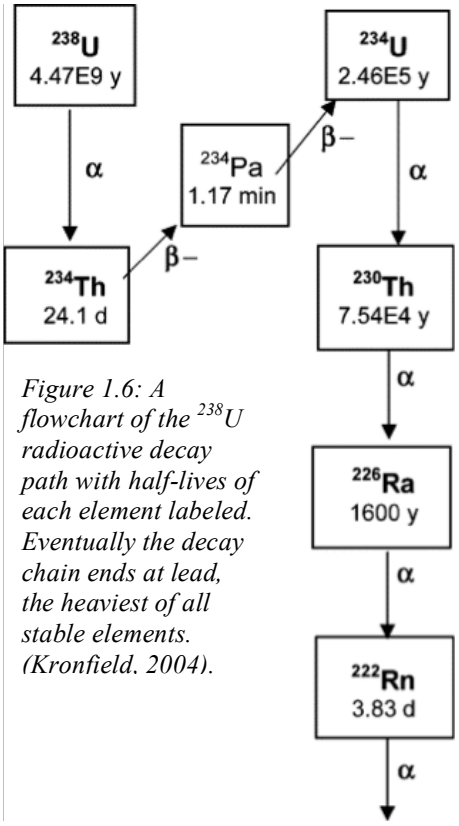

Figure 1.6: A flowchart of the ^{238}U radioactive decay path with half-lives of each element labeled. Eventually the decay chain ends at lead, the heaviest of all stable elements. (Kronfield, 2004).

^{222}Rn measurements of the sea surface water and sedimentary porewater, in situ sea surface salinity and temperature, depth, and wind speed data are used to quantify the sinks and sources of ^{222}Rn. Diffusion rates from sediments where radon is produced by the radioactive decay of ^{226}Ra and offshore contributions from rising tides are considered sources that need to be subtracted out, whereas evasion rates of ^{222}Rn to the atmosphere and offshore removal during falling tides are considered sinks that need to be added to the observed inventory to calculate the original ^{222}Rn flux to the overlying ocean that is SGD derived (for a more detailed description, see calculation procedures in §2.2).

CHAPTER 2

METHODS AND MATERIALS

2.1 Regional Scale Thermal Infrared Remote Sensing

2.1.1 Data Collection

Sea surface temperature (SST) was recorded using high-resolution (2.0 to 3.2 m) aerial infrared thermography (Kelly et al., 2013). A FLIR Systems Inc. (Portland, Oregon) Photon 320 uncooled microbolometer array camera, temperature-adjusted blackbody with a flat-panel design, and combined inertial navigational system and GPS (C-MIGITS II; BEI Systron Donner Inertial Division) were installed in a hole in the fuselage of a twin engine Piper Navajo airplane using a custom-built camera mount. The blackbody was used at three different temperatures (17, 23, and 35ºC) to calibrate all the TIR images while in flight before and after each flight track.

Data were collected at an altitude of 7,000 ft (2,134 m) on June 7th, 2009 during low tide (-0.5 ft) and mostly cloud-clear conditions. The flight was conducted between the hours of 02:00 – 04:00 Hawaii Standard Time (HST) to avoid the effects of solar heating on the SST signatures. In preparation for data collection, three in situ thermistors (HOBO pendant UA-001-08) were deployed within the flight track, anchored to a recorded location, and floated buoyantly at the water's surface. The thermistors were deployed far from seawalls, mangroves, and overhanging trees to ensure that their recorded temperatures would correlate with identifiable points in the image. They were programmed prior to deployment to continuously record SSTs in five-minute intervals and were recovered shortly after the aerial TIR data were collected.

2.1.2 Image Processing

The TIR map constructed in this study was from TIR data collected by Kelly et al. (2013) and the methodology utilized in the data analysis and map preparation was derived from Kelly et al.'s study (2013) as well (see Figure 2.1 for a simplified

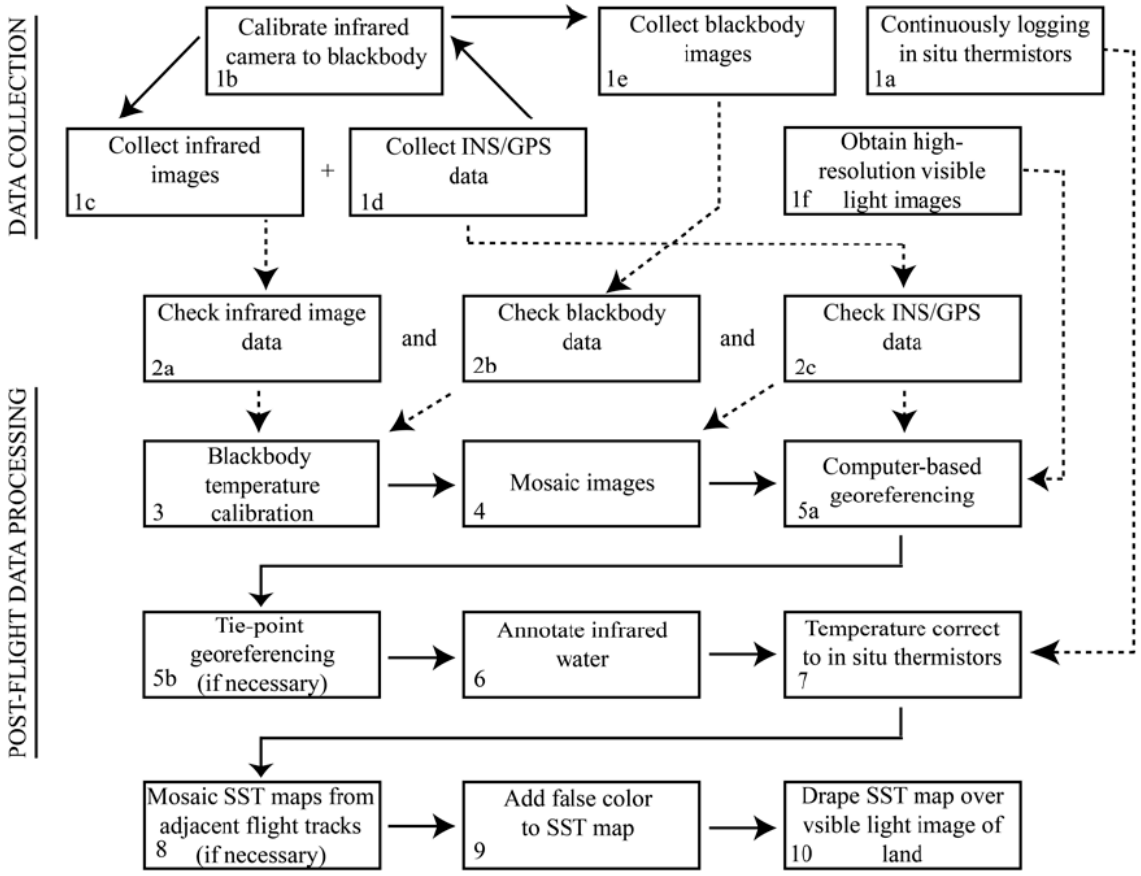

Figure 2.1: Thermal infrared image processing flowchart from Kelly et al., 2013

illustration of the process). The temperature data collected from the flight were first exported to Interactive Design Language (IDL) and corrected to the blackbody on the plane during the flight for three different temperatures (17, 23, and 35ºC). Once calibrated, every third frame was exported to Environment for Visualizing Images (ENVI) and mosaicked into a complete TIR image of the bay. Using ENVI, 0.3 m-resolution georectified visible-light spectrum orthoimages from the United States

Geological Survey were mosaicked together for the area around Kahana Bay. This visible light spectrum image and the GPS data collected on the flight were used to georeference the TIR image. To ground-truth the temperature data and account for atmospheric interference, three HOBO Pendant temperature Data Loggers were deployed to float on the coastal surface waters at fixed GPS points along the flight track prior to the flight. Differences were calculated between each HOBO-recorded temperature at the time of the fly over and their respective pixel in the TIR image. These three differences were then averaged together to produce a thermistor-calibration factor, which was subtracted from every pixel in the TIR image to correct for atmospheric interference.

To construct the final image, the georectified, blackbody, and thermistor-calibrated temperature data of the bay were annotated from the image using ENVI to exclude the land and cloud cover. This annotated image was then exported to ArcGIS and false coloring was applied to best illustrate the temperature variability within the bay. A colorbar was added to act as a legend for the coloring in the image. The mosaic of visible light spectrum satellite images from the USGS was then imported to ArcGIS and laid under the annotated temperature image to produce the final image.

2.2 ^{222}Rn as a Geochemical Tracer of SGD

2.2.1 Spatial Assessment of SGD in Kahana Bay

To determine the spatial distribution of ^{222}Rn throughout Kahana Bay's surface waters, a survey around the perimeter of the bay was conducted on April 20, 2012 from 14:00 – 16:35 (depicted in Figure 2.2). In preparation for the survey, a small, man-powered dinghy was outfitted with monitoring equipment: an electronic radon detector (Durridge RAD7), air/water exchanger, battery-powered bilge pump, multiparameter

water quality probe (YSI V2-4, Sonde), and a battery-powered handheld GPS (Garmin etrex). The RAD7 was connected to an onboard power supply and an air/water exchanger (RAD-AQUA).

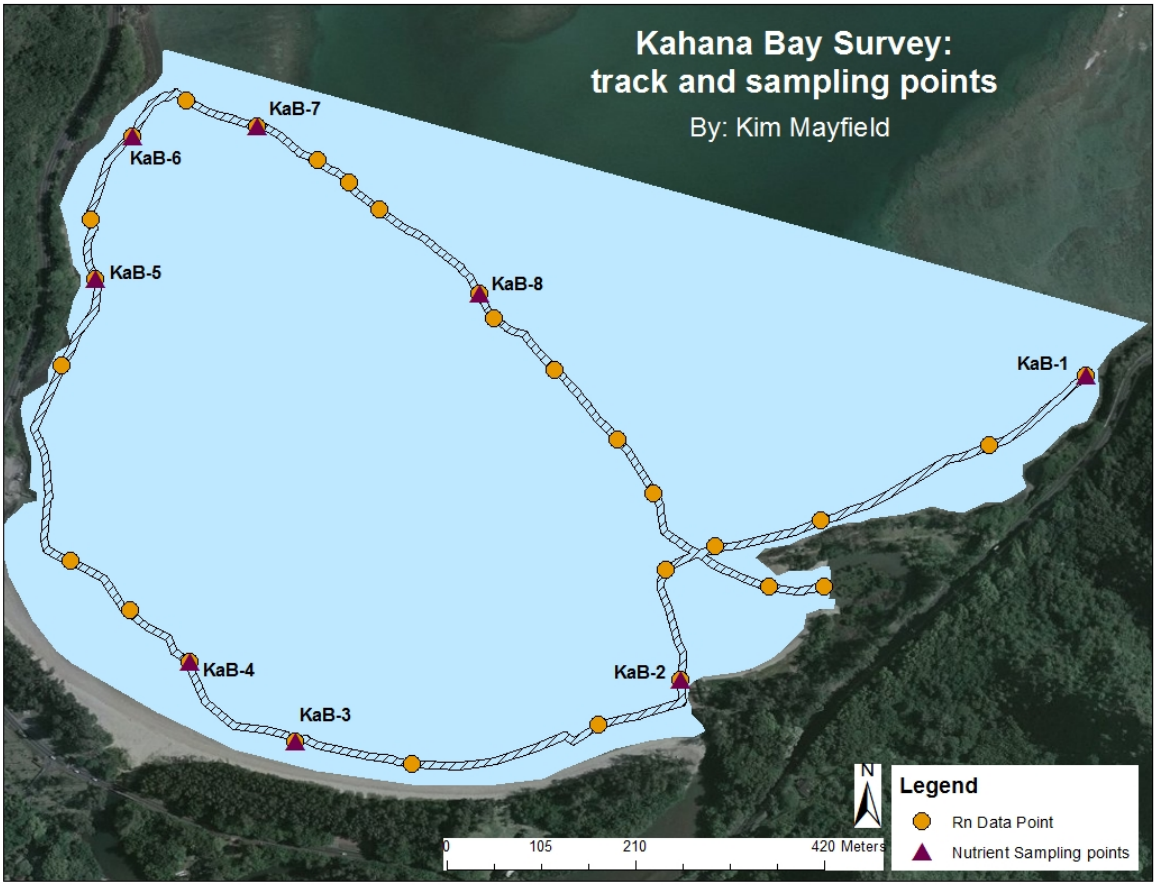

Figure 2.2: A map depicting the survey track taken around the periphery of Kahana Bay on 4/20/2012 from 14:00 – 16:35 with ^{222}Rn data points labeled as orange circles and nutrient sampling points labeled as purple triangles.

The purpose of the air/water exchanger was to de-gas ^{222}Rn from water to the air phase and feed the ^{222}Rn-rich air into the RAD7. The air/water exchanger was fed by a bilge pump, whose head was constantly submerged at 0.2 m depth from the water surface. The RAD7 was set to "sniff mode" to record ^{222}Rn activity in 5 minute intervals. The YSI was programmed to record temperature (ºC), conductivity (mS/cm), salinity, pH, Chl (ug/L), dissolved oxygen (% and mg/L), and turbidity (NTU) every 30 seconds throughout the course of the survey. After programming, the YSI was tethered

horizontally, parallel to the water's surface, along the bow side of the dinghy so that all of the probes were constantly submerged in water. The GPS was set to record position according to the WGS84 datum every 30 seconds throughout the duration of the survey. To assure good spatial resolution, the dinghy was rowed around the perimeter of Kahana Bay at a slow speed, which averaged 1.6 km/hr. The entire survey took approximately 2.5 hours and covered the entire perimeter of the bay.

In addition to a survey of ^{222}Rn in the surface water of Kahana Bay, five groundwater samples were taken to serve as end members: one from a covered, open hole well in Kahana Valley, one from a freshwater spring near the Huilua Fishpond, and three porewater samples taken from the sandy sediments along two sides of Huilua Fishpond and the beach park (see Figure 2.3 for sampling locations).

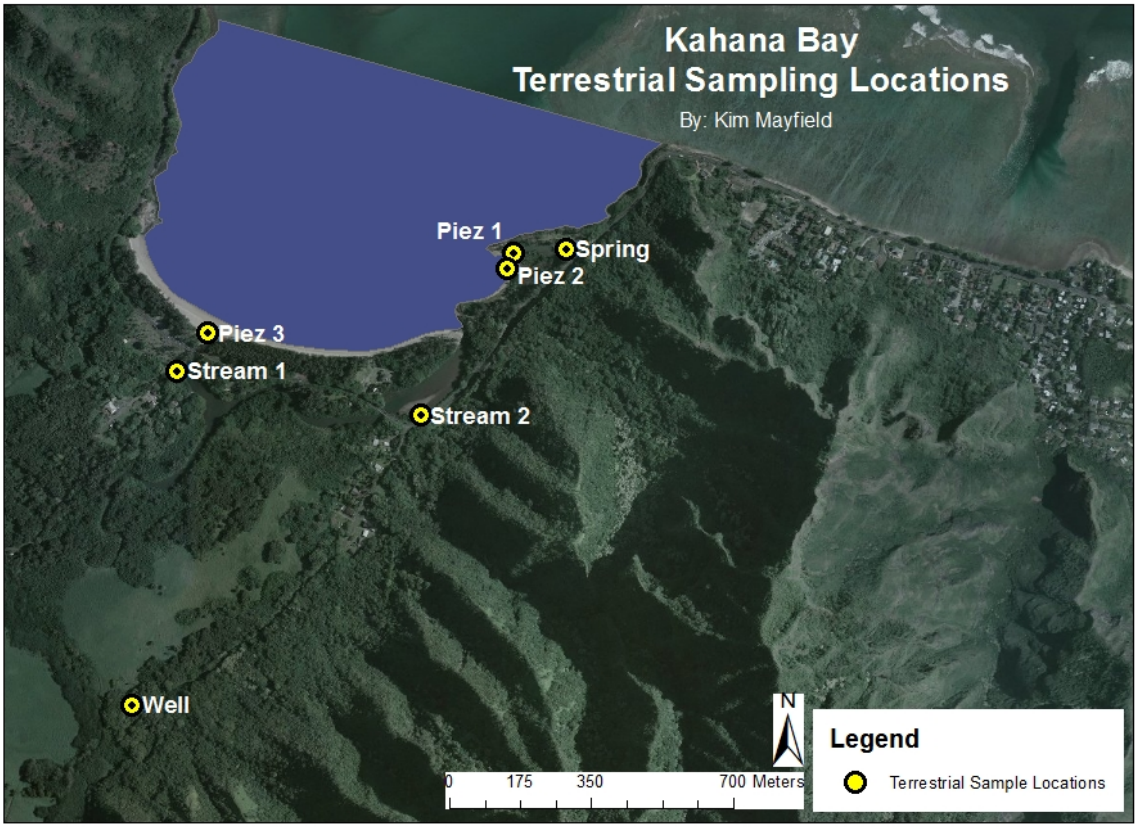

Figure 2.3: A map depicting the terrestrial water sampling locations with their sample ID.

The latter three samples were collected using push point piezometers from the shallow aquifer. Groundwater ^{222}Rn concentrations ranged from 2 – 73 dpm/L, but the upland well sample (73 dpm/L) was chosen to represent the $^{222}Rn_{porewater}$ value because its ^{222}Rn concentration was representative of the Holocene Alluvium that drains the inner bay, as calculated by Garrison et al. (2003).

^{222}Rn counts in the air from the air/water exchanger were measured by the RAD7 in Bq/m^3. Using in situ temperature and salinity, they were converted into dissolved Rn^{222} concentrations in the water using methods described by Schubert et al. (2012).

In ArcMAP, the inverse distance weighted (IDW) algorithm was used to interpolate the ^{222}Rn concentrations in the surface water between data points along the survey track (shown in Figure 2.4). Rectangular delineations were made to surround areas of elevated ^{222}Rn concentrations (see plumes, labeled 'KaB 1' – 'KaB 6,' in Figure 3.2) to define groundwater plumes and account for their ^{222}Rn inventory. ^{222}Rn concentrations in the surface water, temperature, salinity, and depth data recorded within each plume delineation were averaged together. These averages were used to calculate the Ostwald solubility coefficient (k), which was used in conjunction with wind speed data and ^{222}Rn in air to estimate the evasion rate of ^{222}Rn across the air-water interface. The ^{222}Rn benthic flux by diffusion from ^{226}Ra decay in the sediments was estimated based on literature values (Corbett et al., 1998). From the time series ^{222}Rn measurements, we determined that ^{222}Rn concentrations vary with tides and ^{222}Rn concentration drops to offshore levels at every higher-high tide, so the coastal bay water has a residence time of 24.8 hours (see Figure 2.4), which was used to calculate average SGD fluxes over the course of a tidal cycle for each plume. The ^{222}Rn fluxes for each plume were then

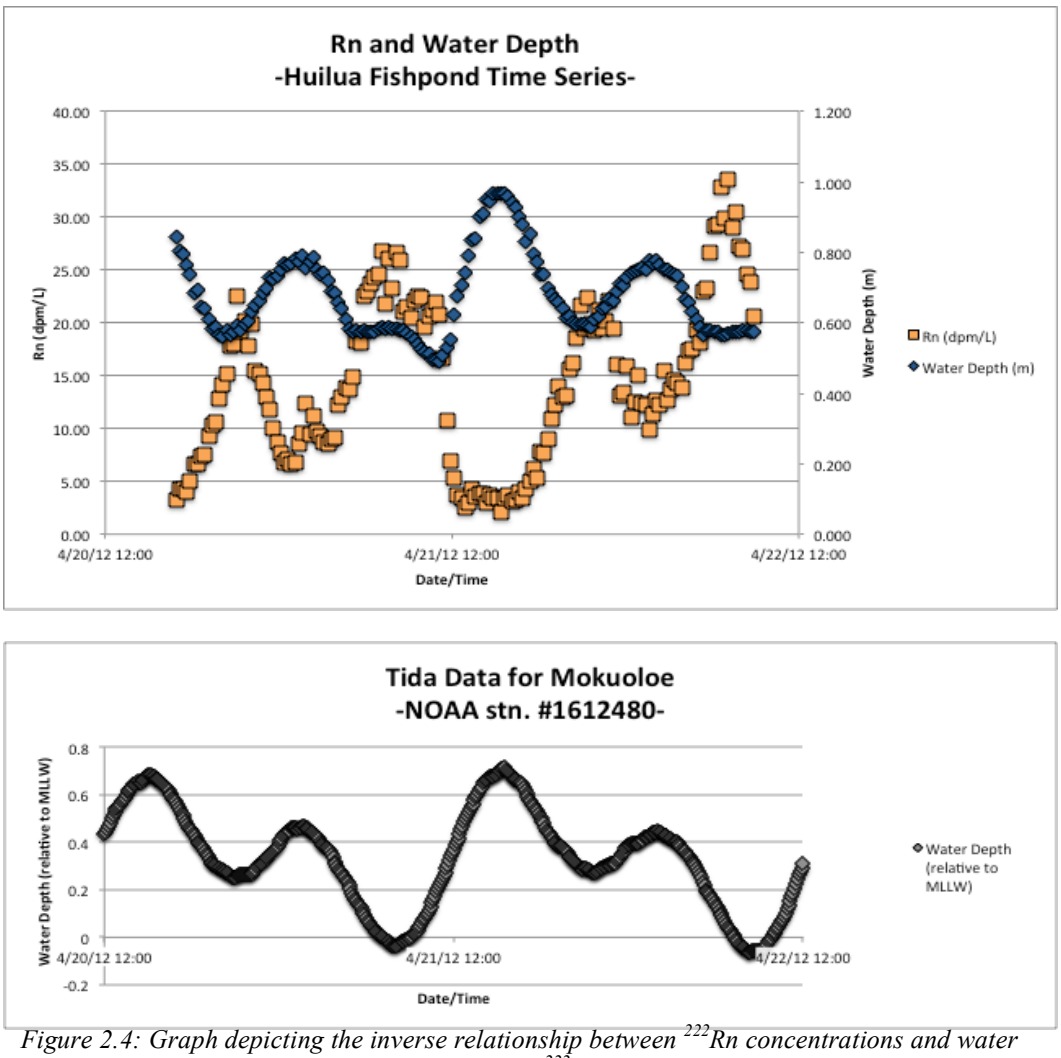

Figure 2.4: Graph depicting the inverse relationship between ^{222}Rn concentrations and water depth in Huilua Fishpond. The residence time of ^{222}Rn in Huilua Fishpond was determined to be one full tidal cycle (24.8 hours) because it's only at the higher-high tide that ^{222}Rn concentrations nearly disappear.

calculated, assuming a steady state of SGD inputs to Kahana Bay over the course of the 2.5 hour survey, the ^{222}Rn in water concentrations were used in conjunction with in situ sea surface salinity and temperature measurements to calculate SGD fluxes via a mass balance model adapted from Dulaiova et al. (2010) (see procedure below).

For each plume:

1) *Diffusion from sediments (D_{sed}) = (sediment radon diffusion from ^{226}Ra concentration/average depth)*(residence time)*

2) *Atmospheric evasion* (E_{atm}) = (((Cw*K)*residence time)/average depth)

3) *Total Rn* ($^{222}Rn_{total}$) = E_{atm} + $[^{222}Rn]_{plume\ avg}$ – $[^{222}Rn]_{offshore}$ – D_{sed} – $[^{222}Rn]_{226Ra}$

4) ^{222}Rn *inventory* ($^{222}Rn_{inv}$) = $^{222}Rn_{total}$*plume area*average depth

5) *SGD Flux* (SGD_{flux}) = $^{222}Rn_{inv}/[^{222}Rn]_{porewater}$

6) $Plume2_{time\ series}$ *% of total SGD flux* = $((SGD_{flux})_{plume\ KaB\text{-}2})/\sum SGD_{flux}$

2.2.2 Temporal Assessment of SGD in Huilua Fishpond

A stationary monitoring platform was set up within the inland side of Huilua Fishpond for one and a half days (35 hours) to observe the temporal variability of SGD. Equipment used for monitoring included an electronic radon detector (RAD7 manufactured by Durridge), air/water exchanger, battery-powered bilge pump, and a multiparameter water quality sonde (YSI 6600 V2-2). An acoustic Doppler current profiler (ADCP) was also deployed in the fishpond next to the stationary platform to record water depth and current velocities at the site every 30 seconds. The RAD7 was programmed to record Rn counts in 15-minute intervals, while the YSI took measurements every 30 seconds.

Data were collected from April 20th, 2012 16:30 (HST) until April 22nd, 2012 09:00 (HST). This time period spanned over an entire tidal cycle, consisting of two high tides (+0.50m and +0.70m) and two low tides (+0.25m and -0.05m) (see Figure 2.4). Conditions were mildly windy with partly cloudy skies and minimal wave action, except for a storm event the morning of April 21st, 2012 between the hours of 07:30 – 11:30. This storm event caused an estimated 2 cm in precipitation, but little change in wind

speeds. Wind speeds during that time recorded between 4.4 – 6.6 m/s (compared to the time series range of 4.4 – 7.5 m/s).

Rn counts in the air from the air/water exchanger were measured by the RAD7 in Bq/m^3. Using in situ temperature and salinity, these values were converted into dissolved ^{222}Rn concentrations in the water using methods described by Schubert et al. (2012). Then, the ^{222}Rn in water concentrations were used in conjunction with in situ sea surface salinity and temperature measurements to calculate the SGD of the time series plume (delineated from the survey) via a mass balance model adapted from Burnett and Dulaiova (2003) (see procedure below).

1) *Ostwald Solubility Coefficient (k) =*

$$e^{(-76.14+(120.36*(100/T))+31.26*\ln(T/100)+(Sal(-0.2631+(0.1673(T/100))+(-0.0273(T/100)^2))))}$$

2) $Cw = [^{222}Rn_{water}] - (k*[^{222}Rn_{air}])$

3) $D_m = 10^{-(1980/T)+1.59}$

4) $S_c = .0086*D_m$

5) $\text{Aeration Constant (K)} = ((0.45(\text{wind speed}^{1.6})(S_c/600)^{-2/3})/100)/60)$

6) $\text{Air-Sea Flux (Evasion}_{atm}) = Cw*K$

7) $\text{Excess } ^{222}Rn \text{ inventory } (^{222}Rn_{excess}) = (([^{222}Rn]_{water} - [^{222}Rn]_{offshore})*depth)$

8) $^{222}Rn_{flux} = \Delta^{222}Rn_{excess} - (^{222}Rn_{excess})_{prior\ reading}$

9) $\text{Ebb tide values (Ebb)} = ^{222}Rn_{excess} - \Delta water\ depth_{15\ min}$

10) $\text{Flood tide values (Flood)} = [^{222}Rn]_{offshore}*\Delta water\ depth_{15\ min}$

11) $\text{Net Flux} = ^{222}Rn_{flux} - Flood + Ebb + Evasion_{atm}$

12) $\text{Mixing Losses: } |^{222}Rn_{flux}|, \text{ if } ^{222}Rn_{flux} < 0$

$$0, \text{ if } {}^{222}Rn_{flux} > 0$$

13) $Total\ {}^{222}Rn_{flux} = {}^{222}Rn_{Netflux} + mixing\ losses$

14) $Advection\ Rate\ (AdvRate) = Total\ {}^{222}Rn_{flux} / [{}^{222}Rn]_{porewater}$

CHAPTER 3

RESULTS

3.1 Spatial Assessment – TIR

As depicted in the June 7th, 2009 TIR map of Kahana Bay (see figure 3.1), sea surface temperatures ranged from approximately 24.5 – 26.9ºC and two cold signatures can be readily identified: a large, diffuse cold signature that characterizes the southern portion of the bay and a northernmost plume, which appears to be diffusing either from the middle of Kahana Bay or along the Punalu'u shoreline. The Punalu`u shoreline along the bay's northwest margin is devoid in riverine inputs and separated from the ocean by an expansive seawall. It isn't certain whether groundwater feeding this SGD plume is being

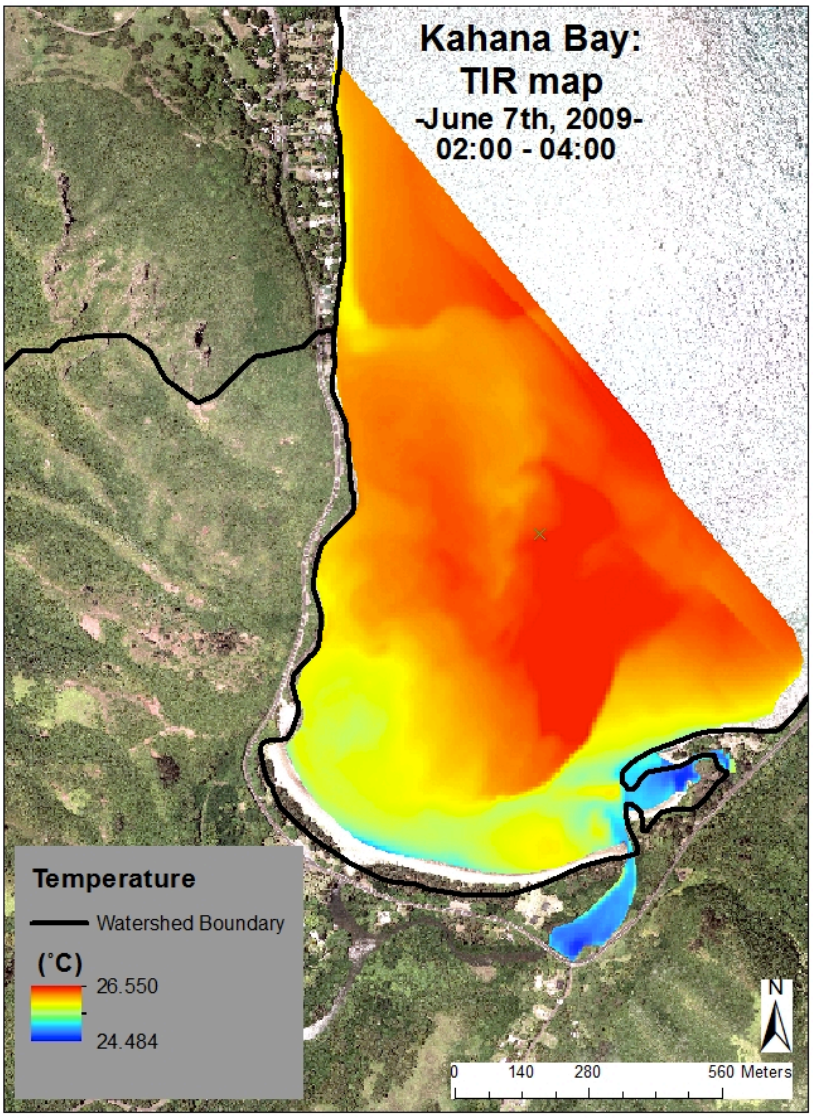

Figure 3.1: TIR map of Kahana Bay

recharged from precipitation within the Kahana or Punalu`u watershed. However, the aquifer recharge for both of these two watersheds comes primarily from orographic rainfall in the Ko`olau Mountain Range, which would result in relatively cool groundwater temperatures, which is assumed to be preserved along the groundwater flow path to the coastline. The diffuse cold signature characterizing the southern portion of the bay can be partially accounted for by stream inputs; however, a large portion of this signature is also likely to be SGD, as evidenced by the radon survey (see below).

3.2 Spatial Assessment

3.2.1 Rn

The concentrations of ^{222}Rn measured in the surface water over the course of the survey ranged from 0.20 – 2.40 dpm/L (Figure 3.2). The highest ^{222}Rn concentrations

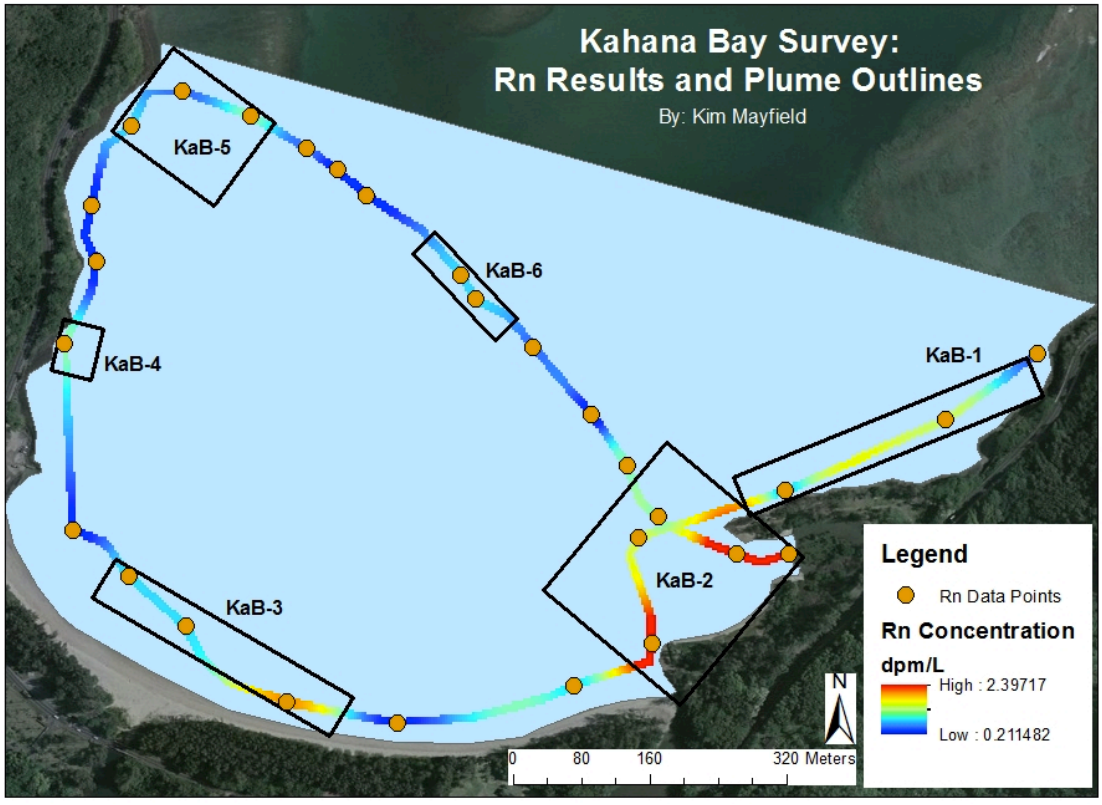

Figure 3.2: Map depicting ^{222}Rn concentrations in the surface waters of Kahana Bay

were located along the southeastern edge of the bay near Huilua Fishpond, along the shoreline to the east of the fishpond, and near the mouths of Kahana River's tributaries. Additionally, Rn concentrations above normal oceanic background levels (~0.5dpm/L) were measured along the western shoreline and in the middle of the bay. After the SGD flux of Plume KaB-2 around Huilua fishpond was divided by the sum of all the plume fluxes of SGD to the bay, the fishpond was found to be responsible for approximately 63% of the total SGD to Kahana Bay at the time of the survey (see below equations, adapted from Dulaiova et al. (2010)).

Final SGD Flux Calculations:

$$Plume_{\text{Time Series}}\ SGD\ Flux = (Area_{\text{Time Series Plume}})*AdvRate_{\text{tidal cycle avg}}$$

$$Kahana\ Bay\ Flux = (Plume_{\text{time series}}\ SGD\ Flux)/(Plume2_{\text{time series}}\ \%\ of\ total\ SGD\ flux)$$

3.2.2 Temperature

The in situ SST data from the survey ranged from 24.49 – 26.89°C and are shown in Figure 3.3, where the data were plotted using the IDW algorithm to interpolate temperatures between the data points. The warmer temperatures (nearly 27°C) were recorded predominantly in the shallow water on the southeastern side of the bay, along the coastline and within the Huilua Fishpond. The coolest surface water temperatures (~24.5°C) were recorded in the middle, deepest part of the bay. These results reflect the SST variability of Kahana Bay during high tide, sunny afternoon conditions in Kahana Bay, which is notably different than the TIR image, which was conducted in the very early morning under low tide conditions (refer to §2.1.1 for details). The decrease in cool

SGD inputs during high tide conditions, combined with the solar heating of the relatively shallow waters along the eastern edge of Kahana Bay and in Huilua Fishpond, obscured the temperatures that would have been expected to match the TIR map.

3.2.3 Salinity

The surface salinity profile of the bay from the survey is shown in Figure 3.4, where the IDW algorithm was used to interpolate salinities between data points. Salinity values ranged from approximately 21 to 35, with the lowest salinities recorded along the beach park edge of Kahana Bay.

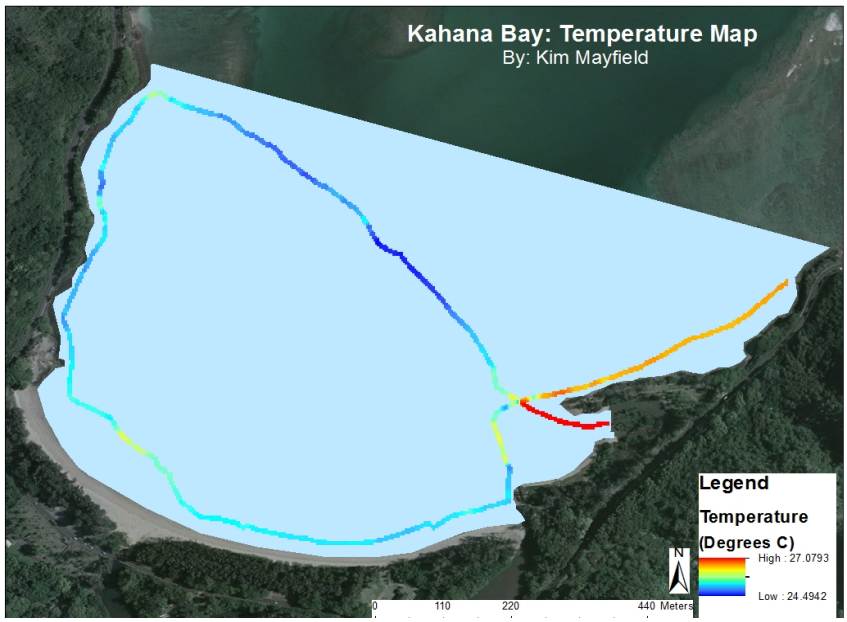

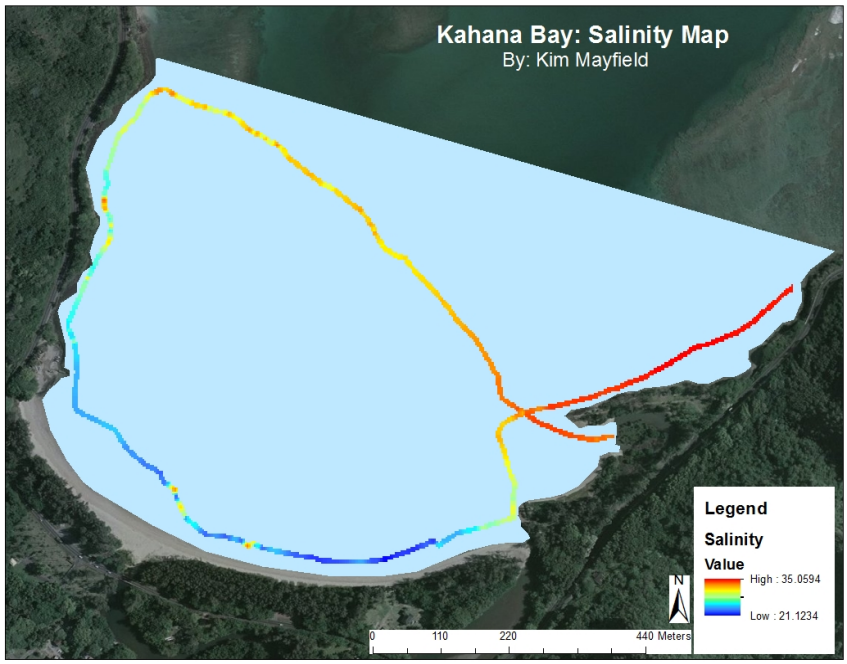

Figures 3.3 (above) and 3.4 (below): Two maps of sea surface conditions in Kahana Bay at the time of the survey on 4/20/12 from 14:00 – 16:35: sea surface temperature (top) and sea surface salinity (bottom).

3.2.4 Nutrient composition

Surface water samples were collected periodically throughout the survey and during two smaller transects across the bay, performed between 10:00 – 11:30 on 4/20/2012 and 09:30 – 11:10 on 4/22/2012. All the samples were analyzed for PO_4^{3-}, $Si(OH)_4$, NO_3^-, NO_2^-, NH_4^+, total P (TP), and total N (TN) (see Appendix, Table A1).

A positive linear relationship exists between the $Si(OH)_4$ and total P, inorganic P, total N, and inorganic N concentrations in all of the marine surface water samples (see Figures 3.5 and 3.6). However, no relationship was discernable between $Si(OH)_4$ and organic P or organic N.

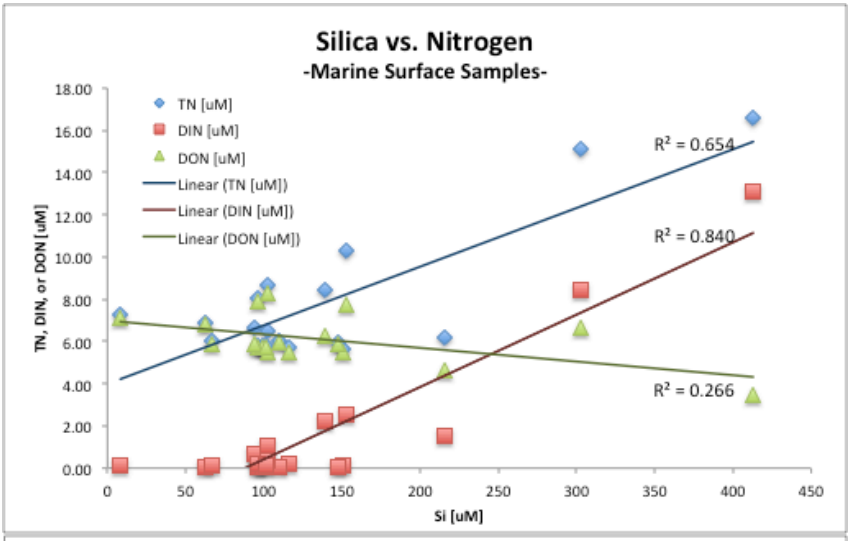

Figure 3.5: Chart depicting the relationships between silica and dissolved nitrogen concentrations in the surface samples of Kahana Bay and Huilua Fishpond.

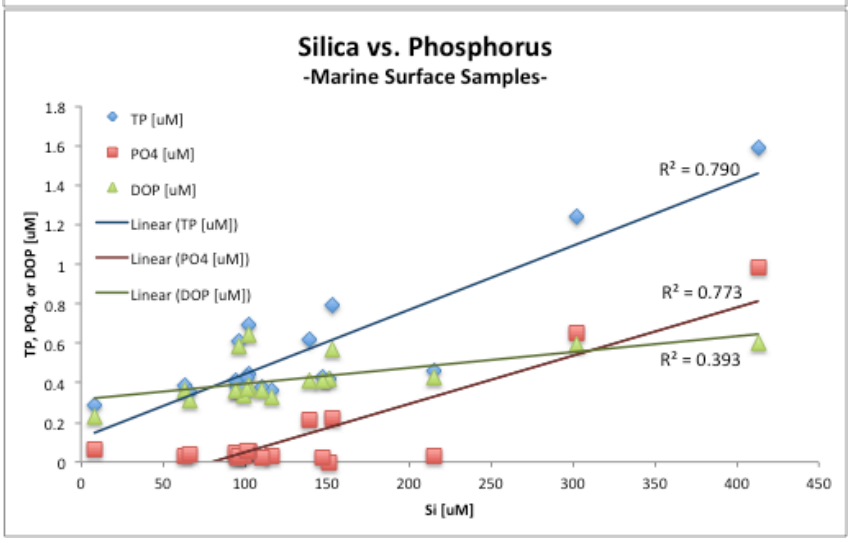

Figure 3.6: Chart depicting the relationships between silica and dissolved nitrogen concentrations in the surface samples of Kahana Bay and Huilua Fishpond.

In the terrestrial water samples, groundwater samples were relatively enriched in dissolved macronutrients, particularly inorganic P and N, with respect to stream samples (see Figures 3.7 and 3.8). Concentrations of $Si(OH)_4$ were comparable between groundwater and stream samples (see Figure 3.9).

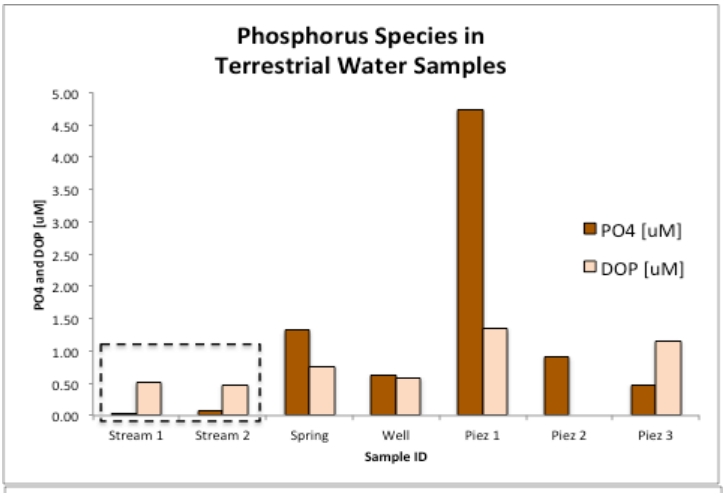

Figure 3.7: Chart depicting PO_4^{3-} and DOP concentrations in the terrestrial water samples collected. Stream samples are highlighted in a dashed outline for comparison to groundwater samples.

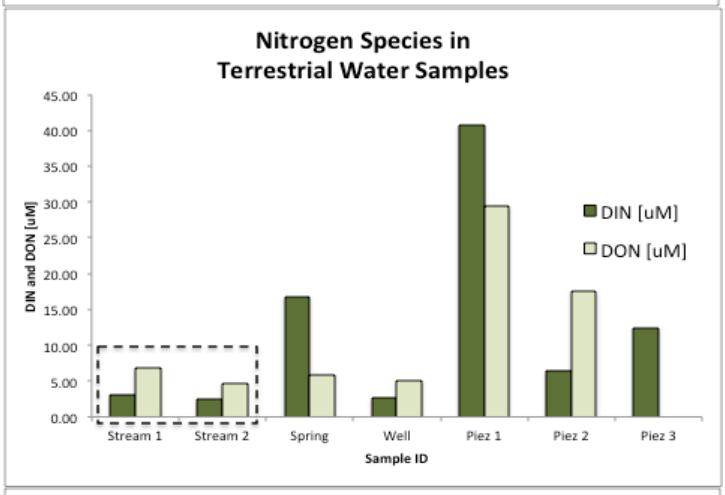

Figure 3.8: Chart depicting DIN and DON concentrations in the terrestrial water samples collected. Stream samples are highlighted in a dashed outline for comparison to groundwater samples.

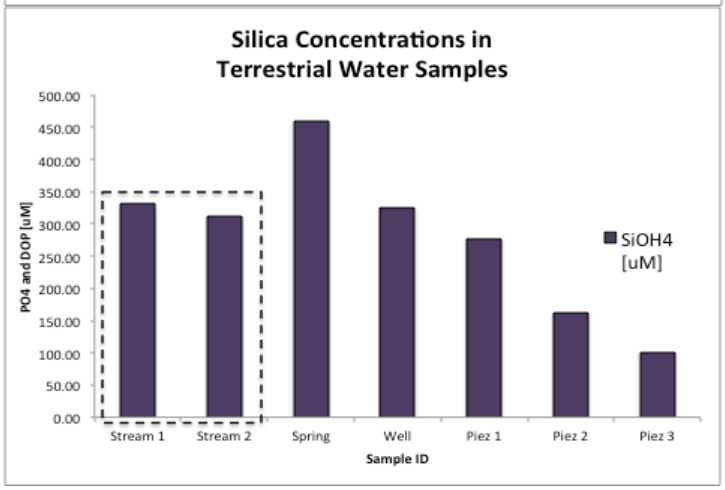

Figure 3.9: Chart depicting $Si(OH)_4$ concentrations in the terrestrial water samples collected. Stream samples are highlighted in a dashed outline for comparison to groundwater samples.

Average nutrient fluxes from the stream were calculated using the two stream water samples taken from two different tributaries of Kahana Stream approximately 50 m upstream from the mouth (see Appendix, Table A2) and the average discharge of Kahana Stream from 4/20 – 4/21/2012 of 54,729 m^3/day (USGS, 2013). The average discharge rate since 2007 (when the stream gauge was first installed) up to our study is 84,816 m^3/day, however, precipitation and stream flow rates in Kahana Valley are highly variable between the wet seasons (winter and spring) and dry seasons (summer and fall). Because this study did not investigate the seasonal variability of SGD to Kahana Bay, the stream flow data from 4/20 – 4/21 were used for all stream flux calculations.

An average groundwater concentration value was calculated for each nutrient species from the five groundwater samples collected (see Appendix, Table A.1). These nutrient concentrations were then multiplied by the average SGD flow rate to yield SGD-derived nutrient fluxes to Kahana Bay. This was done under the assumption that nutrients do not undergo biogeochemical transformations in the aquifer along their flowpath from the well to the coastline. This we believe is met for all piezometer samples as these were collected at the coastline. SGD-derived nutrient fluxes were then divided by stream-derived fluxes to produce SGD/stream nutrient flux ratios (see Appendix, Table A.2).

3.3 Temporal Assessment

3.3.1 Rn

Figure 2.4 clearly illustrates an inversely proportional relationship between water depth and observed ^{222}Rn concentrations, which reflects the tidal influence on SGD dynamics in Kahana. During the time series, inverse linear relationships were observed

between ^{222}Rn concentrations and salinity, as wells as ^{222}Rn concentrations and pH (see Figures 3.9 and 3.10).

The advection rates of SGD for each 15 min time interval during the course of the time series were calculated using a radon mass balance model after Burnett and Dulaiova (2003). The average advection rate over the course of an entire tidal cycle during the time series was multiplied by the plume area (see 'Plume KaB-2' in Figure 3.2) to yield an

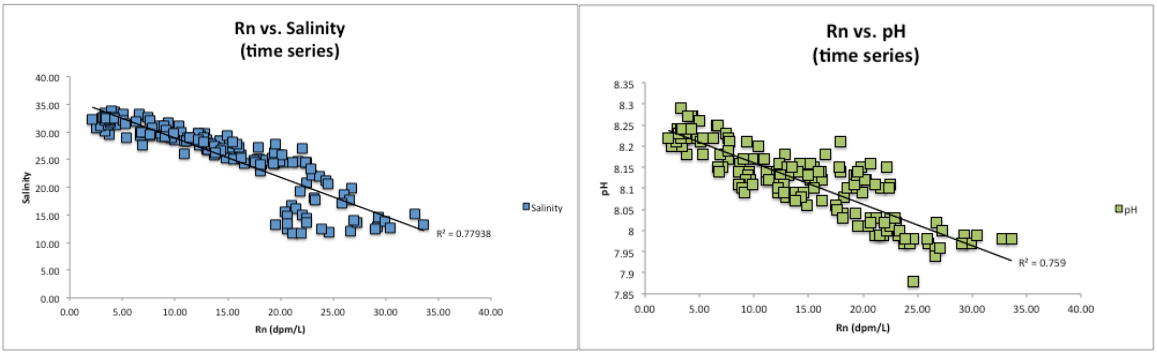

Figure 3.10 (left) and Figure 3.11 (right): graphs demonstrating observed relationships between ^{222}Rn concentrations over the course of the time series.

average discharge rate of 39,796 m^3/day. As calculated earlier in §3.2, Plume KaB-2 is responsible for approximately 63% of the total SGD to the bay. Therefore, the tidal average SGD rate was divided by 0.63, which estimates a total SGD flux to the bay of 62,736 m^3/day.

3.3.2 Salinity

The salinity values recorded over the course of the time series ranged from 11.64 to 33.79, with an average salinity of 26.94 over the course of one full tidal cycle. Assuming a two end member system and an average seawater salinity value of 35, a ratio of marine water to terrestrial groundwater can be calculated using a mixing calculation, the total volume of Huilua Fishpond (34,943 m^3, as defined by the average depth and area of Plume KaB-2 in Figure 3.2), and the salinity values of both end members.

$$Salinity_{avg} = x\,(Salinity^{GW}) + (1 - x)\,(Salinity^{SW})]$$

$$x = (Salinity_{avg} - Salinity^{SW}) / (Salinity^{GW} - Salinity^{SW})$$

Using 26.94 as the average salinity of one full tidal cycle ($Salinity_{avg}$), 35 as the seawater salinity end member of Huilua Fishpond ($Salinity^{SW}$), and 0.15 as the salinity of the terrestrial groundwater end member ($Salinity^{GW}$), the percentage of water in Huilua Fishpond comprised of fresh terrestrial groundwater is approximately 23%. However, we believe this to be an overestimation because even at the highest high tide, when ^{222}Rn concentrations were near background levels, the salinity of Huilua Fishpond only dropped to 33.79.

CHAPTER 4

DISCUSSION

The methodology used to construct the TIR map of Kahana Bay in this study, adapted from Kelly et al. (2013), produced one of the highest resolution coastal TIR images available in published literature to date. Before this study was conducted, no aerial TIR imagery of Kahana Bay existed and the only spatial data on SGD available was from Garrison et al. (2003). Even though the TIR map was constructed using TIR data from a flight in July of 2009 and the field survey of Kahana Bay was conducted in April of 2012, elevated ^{222}Rn concentrations were found in plumes identified by the TIR imagery and were similar to the findings of Garrison et al. (2003). This attests to the consistency of SGD locations within Kahana Bay across lengthy timescales.

The most notable potential groundwater plume noted in the TIR map was certainly the cold signature around Huilua Fishpond, which suggested that it might be the largest source of groundwater to the bay. The results of the ^{222}Rn surface water survey is in agreement with this hypothesis, estimating the plume around Huilua Fishpond to account for approximately 63% of Kahana Bay's SGD inputs. This is an important finding because Garrison et al.'s (2003) study had only estimated the SGD flux to the bay using grounded seepage meters through the bay's floor, but excluded the fishpond from these measurements. The total SGD flux calculated in this study for the inner bay was slightly less than Garrison et al.'s (2003) value, but this can be attributed to the improved accuracy of SGD flux calculations from geochemical tracer studies in the surface waters relative to seepage meters on the sea floor (Burnett & Dulaiova, 2003; Mulligan &

Charette, 2006). This information provided from this study attests to the importance of Huilua Fishpond for the chemical and biological nature of Kahana Bay.

In addition to the plume around Huilua Fishpond, the other plume extents and locations also agreed well with the results of the ^{222}Rn survey. These plumes include the expansive cold signature along the southern edge of the bay by Kahana Beach Park and the diffuse ^{222}Rn signature that was measured along that same part of the shoreline. Additionally, elevated ^{222}Rn signatures correlated well with the locations of the most northwestern plume, above the boat ramp on the western side of the bay, and the mid-bay plume identified in the TIR map. We hypothesize that the mid-bay plume extends from the paleochannel in Kahana Bay north toward Punalu`u based on the TIR map, similar to results of Garrison et al. (2003), and the elevated ^{222}Rn signature found in the survey.

In previous studies conducted by Danielescu et al. (2009) and Kelly et al. (2013), linear relationships were determined between the areas of plumes in the TIR image and the estimated volume of discharge. Unfortunately, the cold signatures in this study's TIR image are relatively diffuse and obscured by inputs from Kahana Stream, which makes clear delineation impossible.

The total volume of Kahana Bay is approximately 20,495,000 m^3, which means that the daily inputs of SGD account for only ~0.3% of the bay's volume. However, cold freshwater inputs appear to account for ~1/3 of Kahana Bay's surface water. Since primary production primarily occurs in the surface waters, we hypothesize that the biological implications of SGD most likely outweigh the volumetric impacts that SGD has on the bay.

The nutrient fluxes calculated in this study (see §3.2.4) also support this hypothesis, since all of the groundwater-derived nutrient fluxes were greater than or equal to Kahana Stream fluxes. The enrichment of inorganic P and N (34:1 and 7:1) in SGD relative to Kahana Stream discharge is of particular interest since these are both macronutrients necessary for biota of the bay. This enrichment is likely because, in the estuarine-like conditions of Hawaiian stream mouths, there are high rates of primary production, which utilize these macronutrients and deplete their concentrations in the river water before it reaches the marine environment. In contrast, SGD bypasses this estuarine filter and its nutrients enter the coastal marine environment directly.

The SGD: stream nutrient flux ratios for Kahana Bay calculated by Garrison et al. (2003) were 5:1, 2:1, and 1:11 for TDP, TDN, and Si, respectively. This study estimated those same ratios to be approximately 5:1, 4:1, and 1:1 respectively. There is a large range with respect to these ratios (as shown in Table 6.1), but the large discrepancy in Si ratios can be attributed to the difference in river flow rates used in this study and Garrison et al.'s (2003). Garrison et al. used a 37-year average flow rate of Kahana River (~90,000 m^3/day), instead of the short time window used in this study's calculations. If the same value is used in conjunction with the data from this study, the ratios of TDP, TDN, and Si are 3:1, 2:1, and 1:2.

In another study, conducted by Knee et al. (2008), in a semi-protected bay on the north shore of Kaua`i (Hanalei Bay) that also receives a lot of orographic rainfall, nutrient flux comparisons between SGD and the watershed's major river, the Hanalei River, were calculated and found to have a widely seasonal range. The minimum SGD: river nutrient flux ratios for PO_4, NH_4^+, Si, and NO_3+NO_2 were as follows: 1:50, 1:100,

below detection, and 1:11 respectively. These minimal ratios were all recorded during February, when the Hanalei River flow rate was very high due to rainy season conditions. The maximum SGD: river nutrient flux ratios of PO_4, NH_4^+, Si, and NO_3+NO_2 (1:7, 1:5, 1:50, and 2.7:1 respectively) were observed in August, when the river flow rate was at a minimum for the study. The remarkable difference in NO_3+NO_2 fluxes was primarily due to fertilizer use on the expansive ponded *kalo* (Colocasia esculenta) agriculture in the area. This comparison shows that groundwater and surface water may play significantly different roles in nutrient delivery to the coast and is greatly influenced by land-use. Kahana Bay is much less agricultural and the stream is not as polluted by coastal development as Hanalei Bay. This field site was still the most applicable to Kahana Bay because the other SGD studies in Hawaii are primarily concentrated around the western coast of Hawai`i Island, which has no stream inputs to the coastlines and drains newly formed, dry lava fields, as opposed to the weathered Holocene alluvium and thick, moist soils of Kahana Bay.

Based on the N:P ratios observed in the marine surface waters of Kahana Bay and Huilua Fishpond, it is likely that the N:P ratio of the primary producers in Kahana Bay is approximately 14:1, which agrees with the N:P ratios of phytoplankton at the Hawaii Ocean Time Series (Neuer et al., 2001) and is slightly lower than the Redfield ratio.

The highest nutrient concentrations in Kahana Bay were observed within the Huilua Fishpond, which supports the hypothesis that terrestrial groundwater is an important source of macronutrients to Kahana Bay's coastal zone. Huilua Fishpond water samples were also the only marine samples with detectable concentrations of NO_2^-, which is an indicator of denitrification pathways under low oxygen levels. The samples that had

detectable concentrations of NO_2^- were from the shallow, murky waters in the back of Huilua Fishpond, by the spring source. These hampered light penetration conditions could hinder photosynthetic rates during the daytime and, when the samples were collected between 10:00 – 11:00 on 4/20/2012, sediments containing organic matter that had undergone respiration under low oxygen conditions could have been resuspended. NO_2^- concentrations decreased with distance from the spring source in the fishpond, which supports this hypothesis.

In addition to nutrient concentrations, groundwater inputs to Kahana Bay were also very well correlated with salinity and pH over the course of the survey. Groundwater in Hawai`i naturally has a lower pH than seawater (the average pH of upland wells in Hawai`i is 7.03 (Hunt, 2004) and the pH of the five groundwater samples collected in this study ranged from 7.07 – 7.22 (with an average of pH of 7.19). The fishpond has significantly lower pH than the ocean in Kahana Bay and this is probably due to discharge of low pH groundwater and because groundwater-derived nutrient delivery increases photosynthesis and respiration of organic matter.

CHAPTER 5

CONCLUSIONS AND FUTURE AVENUES OF RESEARCH

The results of this study clearly indicate that TIR remote sensing is a powerful tool for constructing a regional-scale impression of SGD. In locations with less stream inputs skewing the temperature signature of the SGD, it is even possible to use the image itself to quantify the flux of SGD (Danielescu et al., 2009 & Kelly et al., 2013). However, in Kahana Bay, where there are large surface water inputs, ^{222}Rn was certainly the most effective tracer of SGD. Had temperature and salinity been the only tracers of SGD applied in this summary, then Huilua Fishpond's SGD inputs would have been overlooked because of the high salinity values on the eastern shore of the bay and solar heating of the shallow waters in Huilua Fishpond during the survey. For future research endeavors, it would be best to conduct ^{222}Rn surveys during low tide conditions. The results of the ^{222}Rn survey that was conducted in this study, however, still agreed well with the spatial distribution results of the TIR map. This indicates that the spatial distribution of SGD to Kahana Bay is fairly consistent since the data for the TIR map were collected three years prior to the survey. ^{222}Rn also demonstrated the expected relationships (from previous studies) with tidal water height fluctuations, salinity, and pH in the time series data. It was also a much more accurate identifier of SGD in the survey data than salinity or temperature.

The SGD flux value calculated using ^{222}Rn as a tracer is 62,736 m^3/day. Salinities in the piezometer samples (24.17, 24.49, and 25.27), indicate that about 30% of the SGD to Kahana Bay is fresh (according to the same salinity mass balance equation in §5.3.2). This means that approximately 18,820 m^3/day of the SGD is fresh in composition. The

'inner bay' flux calculated by Garrison et al. (2003) was 78,000 m^3/day, of which 16% (12,480 m^3/day) was derived from the terrestrial aquifer. The boundaries of this study do not extend to the area designated by Garrison et al. as 'mid-bay,' however, their study estimated that the inner bay was responsible for approximately 90% of the total SGD to Kahana Bay, which means that we may have captured the dynamics of the majority of Kahana Bay's SGD in this study. Additionally, Huilua Fishpond was not included in the research scope of Garrison et al.'s (2003) study, which we calculate is responsible for ~63% of the total SGD flux to the bay. The volumetric flux of SGD to Kahana Bay calculated by this study, as well as the results from Garrison et al., were based upon marine-based studies and yielded estimates much larger than the terrestrial-based studies conducted by Takasaki et al. (1969), 38,000 m^3/day, and Lau (1973), 4,000 m^3/day. This is because geochemical tracers derive total SGD, including salty recirculated seawater, brackish, and freshwater discharge from the aquifer, as long as it has remained within the aquifer long enough to equilibrate to the local geology and its ^{222}Rn signature.

Of the total volumetric flux of SGD to Kahana Bay, 63% of which was derived from the Huilua Fishpond plume. Even though organic nutrient fluxes (N and P) were predominantly greater in stream inputs to Kahana Bay than SGD, the inorganic nutrient (N, P, and Si) fluxes of SGD were consistently greater than or equal with respect to Kahana Stream. These inorganic nutrient fluxes led to particularly nutrient rich waters within the Huilua Fishpond.

It is clear that the Kahana watershed has a wealth of hydrologic resources and that Huilua Fishpond is certainly one of its most unique features and an important source of nutrients to the ecosystem of the bay. Historic Hawaiian fishponds were traditionally

constructed around locations of freshwater discharge, such as freshwater springs or streams mouths. The reason for this was that *`Ama`ama* (mullet) and *Awa* (milk fish), the primary species of a Hawaiian fishpond, grow ideally in mixohaline conditions. These two species were selected because they feed directly on the algae within the pond, thereby increasing the efficiency of the energy transfer from the primary producers of the fishpond to the village who later consumed the fish (Devaney, 1976). We recommend that the locations of fishponds in coastal environments be considered when planning an SGD study in the future because they will likely be responsible from an important fraction of the SGD based on this study's results and the results of SGD studies on the west side of Hawai`i Island (Duarte et al., 2006 and Knee et al., 2010).

A follow-up study to investigate the seasonal variability of SGD to Kahana Bay and its role in the bay's primary production would be an asset to the community. Additionally, it would be interesting to analyze the water samples for DIC, POC, DOC concentrations and compare the C : N : P ratios to the Redfield ratio and ratios derived from datasets closer to Hawaii. If a longer time series were conducted that monitored primary production, biomass, and ^{222}Rn concentrations as a tracer for SGD, then a possible relationship between the nutrients derived from SGD and the bay's biota might be observed. Another interesting line of inquiry could be into the variability of the primary producing biota that inhabit the Huilua Fishpond versus the marine environment of Kahana Bay. It is possible that, because of the unusual nature of the Huilua Fishpond's mixohaline and relatively eutrophied, the phytoplankton community could be very different from the marine populations.

Table A.1: Nutrient and 222Rn concentrations of terrestrial and marine samples

	LAT	LON	Rn	[PO_4]	[Si(OH)4]	[NO_3]	[NO_2]	[NH_4]	[TP]	[TN]	DOP	DON
Sample ID	(dec. deg.)	(dec. deg.)	(dpm/L)	[uM]	[uM]	[uM]	[uM]	[uM]	[uM]	[uM]	[uM]	[uM]
stream1	21.5554	-157.8754	9.84	0.04	330.93	1.67	0.04	1.43	0.55	9.92	0.52	6.78
stream2	21.5544	-157.8700	3.69	0.07	311.54	1.26	0.04	1.17	0.54	7.10	0.47	4.63
spring1	21.5581	-157.8667	51.65	1.32	459.81	15.68	0.02	1.07	2.08	22.67	0.76	5.89
well1	21.5480	-157.8764	73.78	0.62	325.11	2.17	0.00	0.43	1.21	7.62	0.59	5.02
piez1	21.5580	-157.8679	2.49	4.74	276.81	0.17	0.02	40.54	6.08	70.15	1.34	29.42
piez2	21.5577	-157.8680	17.79	0.90	162.72	0.50	0.05	5.86	0.66	23.96	-0.24	17.54
piez3	21.5562	-157.8747	4.94	0.47	100.25	0.16	0.02	16.46	1.61	12.46	1.14	-4.18
1	21.5600	-157.8652	0.40	0.06	8.34	0.01	0.03	0.08	0.29	7.26	0.23	7.15
2	21.5569	-157.8693	1.95	0.03	215.80	0.60	0.00	0.92	0.46	6.17	0.43	4.65
3	21.5563	-157.8731	1.47	0.00	151.01	0.04	0.00	0.09	0.42	5.61	0.42	5.47
4	21.5571	-157.8742	0.66	0.02	147.51	0.00	0.00	0.08	0.43	5.97	0.42	5.89
5	21.5609	-157.8751	0.22	0.03	116.00	0.00	0.00	0.23	0.36	5.73	0.34	5.50
6	21.5624	-157.8748	0.65	0.02	110.13	0.03	0.00	0.04	0.38	6.05	0.36	5.98
7	21.5625	-157.8735	0.87	0.02	95.76	0.00	0.00	0.05	0.38	5.77	0.36	5.71
8	21.5608	-157.8713	0.65	0.03	62.85	0.00	0.00	0.08	0.39	6.86	0.36	6.78
pp1-1	21.5577	-157.8671	N/A	0.98	412.82	11.83	0.03	1.27	1.59	16.58	0.61	3.46
pp1-2	21.5580	-157.8670	N/A	0.65	302.39	7.63	0.06	0.73	1.24	15.09	0.59	6.67
pp1-3	21.5578	-157.8679	N/A	0.22	153.02	1.80	0.02	0.75	0.80	10.28	0.58	7.72
pp1-4	21.5578	-157.8685	N/A	0.21	138.96	1.80	0.02	0.37	0.62	8.47	0.40	6.28
pp1-5	21.5578	-157.8701	N/A	0.04	66.74	0.10	0.01	0.04	0.35	6.01	0.31	5.86
pp1-6	21.5582	-157.8729	N/A	0.03	99.37	0.03	0.00	0.04	0.37	5.81	0.34	5.73
pp2-1	21.5587	-157.8710	N/A	0.05	94.09	0.40	0.00	0.30	0.41	6.61	0.36	5.91
pp2-2	21.5591	-157.8718	N/A	0.06	102.37	0.55	0.00	0.48	0.44	6.53	0.39	5.49
pp2-3	21.5595	-157.8729	N/A	0.06	102.18	0.00	0.00	0.37	0.70	8.67	0.64	8.30
pp2-4	21.5590	-157.8743	N/A	0.03	96.43	0.11	0.00	0.07	0.61	8.07	0.59	7.88
pp2-5	21.5589	-157.8750	N/A	0.06	101.80	0.00	0.00	0.12	0.43	5.81	0.37	5.69

Table A.2: Nutrient flux ratios between surface and groundwater samples in Kahana.

	Nutrient Flux Values								
	[PO_4]	[Si(OH)4]	[NO_3]	[NO_2]	[NH_4]	[TP]	[TN]	DOP	DON
ID	[moles/day]	[moles/day]	[moles/day]	[moles/day]	[moles/day]	[moles/day]	[moles/day]	[moles/day]	[moles/day]
Stream1	1.96	18111.34	91.64	2.10	78.32	30.17	543.00	28.21	370.95
Stream2	3.93	17050.02	69.17	2.13	63.82	29.80	388.45	25.87	253.33
Spring1	82.66	28846.32	983.91	1.31	67.15	130.66	1422.16	47.99	369.80
Well1	39.15	20395.99	136.38	0.00	27.00	75.87	478.18	36.72	314.80
Piez1	297.37	17365.69	10.70	0.96	2543.31	381.72	4400.87	84.36	1845.89
Piez2	56.59	10208.36	31.63	3.36	367.57	41.33	1503.14	B.D.	1100.59
Piez3	29.37	6289.27	10.14	1.51	1032.63	101.19	781.88	71.82	B.D.
	Stream Range								
Max	3.93	18111.34	91.64	2.13	78.32	30.17	543.00	28.21	370.95
Min	1.96	17050.02	69.17	2.10	63.82	29.80	388.45	25.87	253.33
Average	2.94	17580.68	80.40	2.11	71.07	29.99	465.73	27.04	312.14
	SGD Range								
Max	297.37	28846.32	983.91	3.36	2543.31	381.72	4400.87	84.36	1845.89
Min	29.37	6289.27	10.14	0.00	27.00	41.33	478.18	0.00	0.00
Median	56.59	17365.69	31.63	1.31	367.57	101.19	1422.16	47.99	369.80
	Comparison of SGD to Stream Nutrient Fluxes								
Conservative Ratio (SGD min/Stream max)	7.48	0.35	0.11	B.D.	0.34	1.37	0.88	B.D.	B.D.
Largest ratio (SGD max/stream min)	151.62	1.69	14.22	1.60	39.85	12.81	11.33	3.26	7.29
Expected ratio (SGD avg/stream avg)	34.32	0.95	2.92	0.68	11.36	4.87	3.69	1.78	2.33

REFERENCES

Akawwi, E., Al-Zouabi, A., Kakish, M., Koehn, F., and Sauter, M. (2008). Using thermal infrared imagery (TIR) for illustrating the submarine groundwater discharge into the eastern shoreline of the Dead Sea – Jordan. *American Journal of Environmental Sciences*, 4(6), 693 – 700.

Brielmann, H., Griebler, C., Schmidt, S. I., Michel, R., and Lueders, T. (2009) Effects of thermal energy discharge on shallow groundwater ecosystems. *FEMS Microbiology Ecology*, 68(3), 273 – 286.

Burnett, W., Bokuniewicz, H., & Huettel, M. (2003). Groundwater and pore water inputs to the coastal zone. *Biogeochemistry*, 66(1/2), 3–33.

Burnett, W. C. and Dulaiova, H. (2003). Estimating the dynamics of groundwater input into the coastal zone via continuous radon-222 measurements. *Journal of Environmental Radioactivity*, 69(1-2), 21 – 35.

Charette, M. A., Moore, W. S., & Burnett, W. C. (2007). Uranium and Thorium-Series Nuclides as Tracers of Submarine Groundwater Discharge, 234–289.

Corbett, D. R., Burnett, W. C., Cable, P. H., and Clark, S. B. (1998). A multiple approach to the determination of radon fluxes from sediments. *Journal of Radioanalytical and Nuclear Chemistry*, 236(1 – 2), 247 – 252.

Costa, O. S., Nimmo, M., & Attrill, M. J. (2008). Coastal nutrification in Brazil: A review of the role of nutrient excess on coral reef demise. *Journal of South American Earth Sciences*, 25(2), 257–270.

Coulbourn, W. T. (1971). Sedimentology of Kahana Bay, O`ahu, Hawai`i. *Hawai`i Institute of Geophysics Report*, 71-14.

Coulbourn, W. T., Campbell, J. F., and Moberly, R. (1974) Hawaiian submarine terraces, canyons, and Quaternary history evaluated by seismic reflection profiling. *Marine Geology*. 17, 215 – 234.

Danielescu, S., MacQuarrie, K. T. B., and Faux, R. N. (2009) The integration of thermal infrared imaging, discharge measurements and numerical simulation to quantify the relative contributions of freshwater inflows to small estuaries in Atlantic Canada. *Hydrologic Processes*, 23(20), 2847 – 2859.

Department of Land and Natural Resources (DLNR). Brochures for Huilua Fishpond and Kahana Bay. Retrieved from: http://www.hawaiistateparks.org/brochures/index.cfm Last accessed: November 1, 2012.

Devaney, D.M., Kelly, M., Lee P. J., and Motteler, L. S. (1976). Kaneohe: a history of change (1778-1950). Prepared for: U.S. Army Corps of Engineers, Pacific Ocean Division, Contract DACW84-76-C-0009. 271 pp.

Duarte, T. K., Hemond, H. F., Frankel, D., & Frankel, S. (2006). Assessment of submarine groundwater discharge by handheld aerial infrared imagery: case study of Kaloko fishpond and bay, Hawai'i. *Limnology and Oceanography: Methods*, 4, 227–236.

Dulaiova, H., Gonneea, M. E., Henderson, P. B., & Charette, M. A. (2008). Geochemical and physical sources of radon variation in a subterranean estuary - implications for groundwater radon activities in submarine groundwater discharge studies. Marine *Chemistry*, 110(1-2), 120–127.

Dulaiova, H., & Burnett, W. C. (2008). Evaluation of the flushing rates of Apalachicola Bay, Florida via natural geochemical tracers. *Marine Chemistry*, 109(3-4), 395–

408.

Dulaiova, H., Camilli, R., Henderson, P. B., and Charette, M. A. (2010). Coupled radon, methane, and nitrate sensors for large-scale assessment of groundwater discharge and non-point source pollution to coastal waters. *Journal of Environmental Radioactivity*, 101(7), 553 – 563.

Garrison, G. H., Glenn, C. R., & McMurtry, G. M. (2003). Measurement of submarine groundwater discharge in Kahana Bay, O'ahu, Hawai'i. *Limnology and Oceanography*, 48(2), 920–928.

Gingerich, S. B., & Oki, D. S. (2000). *Ground water in Hawaii*. US Department of the Interior, US Geological Survey.

Hunt, C. D. (1996). Geohydrology of the island of O'ahu, Hawai'i. U.S. Geological Survey Professional Paper 1412-B.

Hunt Jr., C. D. (2004). Ground-water quality and its relation to land use on Oahu, Hawaii, 2000-01. Natinonal Water-Quality Assessment Program, USGS Report 03-4305.

Johannes, R. E., & Hearn, C. J. (1985). The effect of submarine groundwater discharge on nutrient and salinity regimes in a coastal lagoon off Perth, Western Australia. *Estuarine, Coastal and Shelf Science*, 21(6), 789-800.

Johnson, A. G., Glenn, C. R., Burnett, W. C., Peterson, R. N., & Lucey, P. G. (2008). Aerial infrared imaging reveals large nutrient-rich groundwater inputs to the ocean. *Geophysical Research Letters*, 35(15), 1–6.

Kelly, J. L., Glenn, C. R., and Lucey, P. G. (2013). High-resolution aerial infrared mapping of groundwater discharge to the coastal ocean. Limnology and Oceanography Methods. (accepted)

Knee, K. L., Layton, B. A., Street, J. H., Boehm, A. B., & Paytan, A. (2008). Sources of nutrients and fecal indicator bacteria to nearshore waters on the north shore of Kaua`i (Hawai`i, USA). *Estuaries and Coasts*, 31(4), 607 – 622.

Knee, K. L., Street, J. H, Grossman, E. E., Boehm, A. B, & Paytan, A. (2010). Nutrient inputs to the coastal ocean from submarine groundwater discharge in a groundwater-dominated system: relation to land use (Kona Coast, Hawaii, USA). *Limnology & Oceanography*, 55(3), 1105 – 1122.

Kronfield, J., Godfrey-Smith, D. I., Johannessen, D., and Zentilli, M. (2004). Uranium series isotopes in the Avon Valley, Nova Scotia. *Journal of Environmental Radioactivity*, 73, 335 – 352.

Lau, L. S. (1973). The quality of coastal water: second annual progress report. University of Hawai`i, Water Resources Research Center Technical Report 77.

Miller, J. A. (1999). *Ground Water Atlas of the United States: Alaska, Hawaii, Puerto Rico, and the US Virgin Islands*. US Geological Survey.

Miller, D. C., and W. J. Ullman. (2004). Ecological consequences of groundwater discharge to Delaware Bay, United States. *Ground Water,* 42: 959–970

Moore, W. (2000). Determining coastal mixing rates using radium isotopes. *Continental Shelf Research*, 20(15), 1993–2007.

Moore, W. S. (1999). The subterranean estuary: a reaction zone of ground water and seawater. *Marine Chemistry*, 65(1-2), 111–125.

Moore, W. S. (2006). The role of submarine groundwater discharge in coastal biogeochemistry. *Journal of Geochemical Exploration*, 88(1-3), 389–393.

Moore, W. S., Sarmiento, J. L., & Key, R. M. (2008). Submarine groundwater discharge

revealed by ^{228}Ra distribution in the upper Atlantic Ocean. *Nature Geoscience*, 1(5), 309–311.

Moore, W. S. (2010). The Effect of Submarine Groundwater Discharge on the Ocean. *Annual Review of Marine Science*, 2(1), 59–88.

Morland, G., Strand, T., Furuhaug, L., Skarphagen, H., and Banks, D. (1998). Radon in quaternary aquifers related to underlying bedrock geology. *Ground Water*, 36(1), 143 – 146.

Mulligan, A. E. and Charette, M. A. (2006). Intercomparison of submarine groundwater discharge estimates from a sandy unconfined aquifer. *Journal of Hydrology*, 327, 411 – 425.

Neuer, S., Davenport, R., Freudenthal, T., Wefer, G., Llinas, O., Rueda, M. J., Steinberg, D. K., Conte, M. H. and D. M. Karl, D. M. (2001). Differences in Redfield ratios between open ocean time series stations and implications for carbon export. ASLO Aquatic Sciences Meeting, Albuquerque, NM, February 2001.

Niencheski, L. F. H., Windom, H. L., Moore, W. S., and Jahnke, R. A. (2007). Submarine groundwater discharge of nutrients to the ocean along a coastal lagoon barrier, Southern Brazil. *Marine Chemistry*, 106(3-4), 546–561.

Rosenau, J. C., Faulkner, G. L., Hendry, C.W., and Hull, R. W. (1977). Springs of Florida. *Florida Bureau of Geology Bulletin*, 31 (revised), 457 – 461.

Schubert, M., Paschke, A., Lieberman, E., and Burnett, W. C. (2012). Air-water partitioning of ^{222}Rn and its dependence on temperature and salinity. *Environmental Science and Technology*. 46(7), 3905 – 3911.

Shaban, A., Khawlie, M., Abdallah, C., & Faour, G. (2005). Geologic controls of submarine groundwater discharge: application of remote sensing to north Lebanon. *Environmental Geology*, *47*(4), 512-522.

Shepard, D. (1968). A two-dimensional interpolation function for irregularly-spaced data. *Proceedings of the 1968 ACM Conference,* 517 – 524.

Stearns, H. T. and Vaksvik, K. N. (1935). Geology and groundwater resources of the island of O`ahu, Hawai`i. Hawai`i Division of Hydrology Bulletin, 1, 479.

Takasaki, K. J., Hirashima, G. T., and Lubke, E. R. (1969) Water resources of Windward O'ahu, Hawai'i. U.S. Geological Survey Professional Paper 1894.

Taniguchi, M., Burnett, W. C., Cable, J. E., and Turner, J. V. (2002). Investigation of submarine groundwater discharge. *Hydrological Processes*, 16(11), 2115–2129.

U.S. Census Bureau. (2012, September 18). State & County Quickfacts: Honolulu, H.I. Retrieved: October 20, 2012, from http://quickfacts.census.gov/qfd/states/15000.html.

U.S. Geological Survey. (2013). Gauge #16296500 Kahana Stream: discharge data. U.S. Department of the Interior/USGS. Retrieved from: http://waterdata.usgs.gov/nwis/uv?cb_00060=on&format=gif_default&period=&begin_date=2013-04-30&end_date=2013-05-07&site_no=16296500

Waska, H., & Kim, G. (2011). Submarine groundwater discharge (SGD) as a main nutrient source for benthic and water-column primary production in a large intertidal environment of the Yellow Sea. *Journal of Sea Research*, 65(1), 103–113.

Zekster, I. S. (2000). Groundwater and the Environment - Applications for the global community. Lewis Publishers, Boca Raton, 175.